Directed growth during somatic cell fusion in *Neurospora crassa* requires contributions from two distinct MAP kinase pathways

Antonio Serrano[1,2] *, Hamzeh H. Hammadeh[1], Ulrike Brandt[1] and André Fleißner[1] *

1 Institut für Genetik, Technische Universität Braunschweig, Spielmannstraße 7, 38106 Braunschweig, Germany

2 Centro de Biotecnología y Genómica de Plantas, Universidad Politécnica de Madrid (UPM)–Instituto Nacional de Investigación y Tecnología Agraria y Alimentaria (INIA/CSIC), Campus de Montegancedo UPM, Pozuelo de Alarcón, Madrid, Spain.

† Present address: Max Planck Institute for Heart and Lung Research, Bad Nauheim 61231, Germany.

* To whom correspondence should be sent: aserrano@csic.es / a.fleissner@tu-braunschweig.de

Summary statement

MAK-1 activates the Rho GTPase RAC-1 to drive actin polymerization, while MAK-2 orients this RAC-1/actin complex toward the fusion partner, defining complementary MAPK roles in somatic cell fusion.

Abstract

Somatic cell fusion in *Neurospora crassa* depends on two MAP kinases, MAK-1 and MAK-2, but their precise contributions to directed growth have remained unclear. Using analog-sensitive alleles and live-cell imaging, we found that MAK-1 activity is required for RAC-1 activation and polarized actin assembly, while MAK-2 controls the positioning of RAC-1 and actin at the fusion tips. Inhibition of MAK-1 disrupted cell communication, prevented actin focus formation, and blocked membrane recruitment of MAK-2 and SO. In contrast, MAK-2 inhibition caused SO and actin to shift to alternative cortical sites, showing that MAK-2 regulates their spatial orientation rather than activation. Actin disruption with latrunculin A eliminated MAK-2 and SO recruitment, confirming its essential role in their localization. Importantly, MAK-1 controlled actin polymerization only during tropic growth, not during general hyphal extension, and acted upstream of RAC-1. These findings establish complementary roles for MAK-1 and MAK-2 in directing RAC-1–dependent actin dynamics during fungal cell fusion.

Introduction

Cell polarization is a fundamental process in eukaryotic organisms, indispensable for growth, development, and certain types of cellular communication. It involves the asymmetric distribution of various molecular factors, including proteins, lipids, and RNA, to discrete regions of the cell cortex, enabling specialized functions at distinct cellular sites. A prominent example of this phenomenon is polarized growth, defined by selective cell expansion at define sites, resulting in elongated morphologies. Examples of cells undergoing highly polarized growth include neurons in animals [1], root hairs and pollen tubes formation in plants [2], and mating protrusions (shmoo) in yeast [3]. Filamentous fungi provide some of the most striking examples of polarized growth, as their hyphal cells extend continuously at the tip and form branched, interconnected mycelial networks capable of rapid and directional exploration of the environment [4-6].

Polarized growth in fungi can be broadly divided into two categories: general polarized growth and directed growth (chemotropic or tropic growth). During general polarized growth, hyphae or the germ tubes of germinating spores protrude continuously in a defined axis, often without changing direction. By contrast, directed growth refers to the reorientation of hyphal tips in response to specific environmental or cellular cues, such as host-derived signals in pathogenic fungi, nutrient gradients, or the presence of a compatible fusion partner. This facilitates cell-cell fusion (somatic fusion) of compatible cells, a pivotal process for colony networking, resource sharing, and the formation of specialized sexual structures [7].

In filamentous fungi, this process of somatic fusion takes place repeatedly throughout development and serves as the basis for building an interconnected colony. Fusion occurs first between germinating spores (germling fusion) and later between mature hyphae (hyphal fusion), establishing cytoplasmic continuity between cells and allowing the exchange of nutrients, signals, and organelles within the mycelial network. Each fusion event follows a defined sequence that includes mutual recognition between compatible partners, chemotropic growth of the cell tips toward one another, and subsequent cell wall remodeling and membrane merger. The recognition and tropic growth phases are driven by a “cellular dialogue,” a dynamic oscillatory communication in which interacting cells alternate between signal-sending and signal-receiving states to coordinate directed growth and ensure successful fusion [8, 9].

A key aspect of understanding how cells translate extracellular cues into polarization is the mitogen-activated protein (MAP) kinase network [10, 11]. This conserved signaling machinery governs multiple facets of polarized growth across diverse organisms. In the baker’s yeast *Saccharomyces cerevisiae*, the Fus3 MAPK pathway is the most studied regulator of mating, wherein cells detect peptide pheromones released by opposite mating type. Upon pheromone

sensing by specific G protein-coupled receptors, a cascade of GTPases and kinases converges on phosphorylation of Fus3p, driving transcriptional changes and orchestrating the reorganization of the actin cytoskeleton at the site of the pheromone gradient. Concurrently, the cell wall integrity (CWI) pathway, centered on the MAPK Slt2/Mpk1, collaborates with the pheromone pathway to ensure proper cell wall remodeling [12] and the control of polarity under mechanical stress [13]. Additionally, the CWI pathway regulates cell wall modifications required for the culmination of the sexual cell fusion process. Tight coordination of both MAPK pathways ensures that membrane extension and cell wall restructuring take place correctly, enabling precise polarize growth toward the mating partner [14]. Related mechanisms governing MAPK-dependent polarization operate in other yeast and fungal species. In the fission yeast *Schizosaccharomyces pombe*, MAPK such as Pmk1 (the CWI pathway homolog to yeast) contribute to cell integrity and polar growth [15]. Similarly, the filamentous fungus *Neurospora crassa* relies on two MAPK modules, the MAK-1 (Mpk1p homolog) and MAK-2 (Fus3p homolog) pathways, for hyphal fusion and colony morphogenesis. Mutants lacking either pathway fail to initiate normal somatic fusion events and cannot form the interconnected mycelial networks of wild-type colonies [16, 17].

Although all fungal hyphae exhibit continuous tip extension (general polarized growth), certain stimuli necessitate a shift to directed growth. In *N. crassa*, vegetative germling fusion requires tropic interactions between germ tube tips. The switch to directed growth involves rearranging the polarity machinery, including classic polarity regulators, such as Rho-type GTPases, including CDC-42 and RAC-1, that govern actin cytoskeleton organization and exocytosis, ensuring the delivery of secretory vesicles to the cell tips [18, 19]. Notably, in this fungus, CDC-42 is essential for sustaining general germ tube extension, while RAC-1 drives the tropic response and directed growth associated with cell fusion events [19]. Both regulators seem to interact with similar downstream components, such as the formin Bni1, that nucleates actin polymerization, and associated filaments form actin cables that enable secretory vesicles delivery to the polarity sites [19].

During this process, the MAPK MAK-2 oscillates between the cytoplasm and the plasma membrane at the tip of the interacting cells, facilitating rapid switches in the cellular dialogue [8, 9]. Meanwhile, the MAPK MAK-1 pathway functions predominantly at later fusion stages and contact recognition, controlling the cell wall remodeling and membrane merger once the fusion partners come into physical contact [20]. However, it is currently unclear, if the MAK-1 pathway also plays any role during directed growth of the fusion cells towards each other.

By delineating temporal and functional roles of these MAPK pathways, we provided a more comprehensive framework for understanding the cellular transition between general and

111 directed polarized growth. By employing a chemical genetics approach with analog-sensitive
112 MAPK variants (*Shokat* alleles) [21, 22], in combination with high spatial resolution live-cell
113 imaging, we demonstrate that MAK-2 is decisive in orienting growth toward the fusion
114 interacting cell, ensuring that RAC-1 (Rho-type GTPase) remain properly polarized to drive
115 precise chemotropic growth. Conversely, MAK-1 is also required for maintaining the polarized
116 state during directed growth and ensuring actin oscillation between the interacting cells. Taken
117 together, our results support a model in which the two MAPK act in tandem during directed
118 polarized growth.

119 **Results**

120 ***Inhibition of MAK-1 kinase activity disrupts the process of cell fusion***

121 The CWI MAPK MAK-1 is known to play important roles in the successful completion of cell
122 fusion, including an essential but unknown role in establishing cell fusion competence, and its
123 activity is crucial for growth arrest of fusing cells after physical contact is established [20, 23].
124 However, it remains unclear whether MAK-1 also plays a role during the tropic interaction of
125 fusion partners. Deletion of the *mak-1* gene completely disrupts cell fusion competence [23],
126 prompting us to create an analog-sensitive version, or *Shokat* allele [21], of MAK-1 to
127 manipulate its activity in a spatial-temporal manner (Fig. S1A and B).

128 The resulting strain, MAK-1^{E104G} (*mak-1::mak-1^{E104G}-hph*), appeared macroscopically wild
129 type-like, indicating that the mutated kinase is functional in the absence of the inhibitor (ATP-
130 analog, 1-NM-PP1) and supplemented with 1% DMSO (the solvent of 1-NM-PP1) as a control
131 (Fig. S1C). In contrast, addition of the inhibitor (final concentration of 40 µM) to the growth
132 medium resulted in a Δ*mak-1*-like phenotype, whereas the wild-type control strain remained
133 unaffected (Fig. S1C). Microscopic analysis showed that the presence of the inhibitor
134 drastically reduced the cell fusion rate of the MAK-1^{E104G} strain, enabling us to analyze the
135 functions of MAK-1 at specific stages of the cell fusion process, such as the cell-cell
136 communication phase (Fig. S1D). Additionally, as previously shown in other publications,
137 neither the solvent DMSO nor the ATP-analog had any effect on wild-type cells, demonstrating
138 the specificity of the inhibitor for analog-sensitive variants in our fungal system.

139 To investigate further the effects of MAK-1 inhibition on cell-cell communication, multiple
140 strains were created. The proteins MAK-2 and SO are crucial to the cell fusion process, and
141 thus, we examined the localization of these following MAK-1 inhibition. The strains MAK-1^{E104G}
142 + SO-GFP and MAK-1^{E104G} + MAK-2-GFP were created through sexual crosses (see Materials
143 and methods for more details). All strains exhibited comparable MAK-1 inhibition
144 macroscopically phenotypes upon the addition of the ATP-analog (data not shown). When

145 live-cell imaging of cell-cell communication, the addition of DMSO did not affect the normal
146 oscillatory recruitment of MAK-2 (Fig. 1A). However, the addition of the ATP-analog
147 completely disrupted the cell-cell communication process, and the dynamic localization of
148 MAK-2 was interrupted. The kinase was no longer observed on the membrane, and no full
149 detachment occurred even after almost 18 minutes (Fig. 1B). Similarly, the addition of DMSO
150 did not affect the usual oscillatory recruitment of SO (Fig. 1C). However, 10 minutes after the
151 addition of the kinase inhibitor, SO accumulated at the membrane in both cell tips, and the
152 GFP signals were more widely distributed around the cell tips (Fig. 1D). These findings
153 suggest that MAK-1^{E104G} activity is essential for proper MAK-2 and SO dynamics during the
154 directed growth phase. Similarly, the characteristic MAK-2/SO dynamics also occur during
155 hyphal fusion [24]. We therefore examined the effects of MAK-1 inhibition on hyphal fusion
156 events. When DMSO was added, MAK-2 oscillated in a wild-type manner (Fig. S2A). However,
157 when MAK-1^{E104G} was inhibited, MAK-2 exhibited a disruption of their dynamics similar to the
158 findings in germlings (Fig S2B). Regarding SO, DMSO did not affect the usual oscillatory
159 dynamics (Fig. S2C), but the addition of the inhibitor completely disrupted the process (Fig.
160 S2D). While MAK-2 completely vanished from the hyphal tip, SO remained as single dots
161 distributed widely around the plasma membrane of both interacting hyphae. These data
162 indicate that the function played by MAK-1 during germling fusion is also conserved in hyphal
163 fusion.

164 Proper actin organization is crucial for polarized hyphal extension in fungi. In non-interacting
165 cells, actin is primarily found at the tips of growing germ tubes in the form of actin patches
166 localized around the cell tips and actin cables [18]. During cell fusion, the disruption of actin
167 assembly leads to a failure of polarized, directed growth of the fusion tips, while microtubules
168 are dispensable for this process [25]. To image actin dynamics, we used the LifeAct reporter,
169 previously adapted for our fungal system [18], and created a strain MAK-1^{E104G} + LifeAct-GFP
170 through a sexual cross (see Materials and methods for more details). This strain behaved
171 similarly to the wild type in the presence of DMSO, and typical actin cables were present at
172 the cell tips during the communication phase and during cell merger, comparable to wild-type
173 cells. Previously unreported in our system, we observed that actin dynamics showed a
174 comparable oscillatory and alternating accumulation at the cell tips of the interacting cells as
175 MAK-2 and SO (Fig. 1E). When MAK-1^{E104G} was inhibited, actin accumulation was clearly
176 affected: the accumulation of actin cables from the tips disappeared and actin patches were
177 no longer focused on the cell tips but localized in a wider distribution around the cell membrane
178 of the entire cell body (Fig. 1F). Actin oscillation was also observed in hyphal fusion, and
179 inhibition of MAK-1^{E104G} disrupted actin accumulation at the hyphal tips, in a similar fashion as
180 described in germlings (Fig. S2E and F).

181 These data indicate that MAK-1 is involved in the regulation of the actin cytoskeleton, MAK-2
182 and SO dynamics during the cell fusion process.

183 ***Actin accumulation at the cell tips oscillates out-of-phase with SO/MAK-2 dynamics.***

184 Remarkably, the observation of actin localization in the presence of DMSO in the MAK-1^{E104G}
185 inhibitable strain suggested that actin accumulates at the cell tips of the interacting cells and
186 that this accumulation oscillates in an antiphase manner (Fig. 1E). To further investigate
187 whether this was a specific effect of this strain, we examined actin localization in wild-type
188 cells. Using the wild-type strain LifeAct-GFP [18], we made the same observations (Fig. 2A &
189 S3A). Based on these data, we hypothesized that actin accumulation likely occurs together
190 with SO, since the presence of SO at the cell tips is associated with a signal sending state of
191 the fusing cell [26, 27]. We therefore created a heterokaryon combining LifeAct-GFP, and
192 dsRed-SO, to enable observation of actin and SO within the same cell. When interacting cell
193 pairs were observed, dynamic interferes co-localization was found, in which SO was recruited
194 to the membrane at the tip of the first pair, while actin was recruited in the second interacting
195 cell. After a few minutes, both proteins co-localized at the tip of the first partner. Finally, actin
196 disassembled from the membrane of the upper cell and was recruited in the lower cell, while
197 SO remained at the tip of the upper cell (Fig. 2B and S3B, C and D). This indicates that actin
198 polymerization at the cell tips is out-of-phase with the usual dynamics of MAK-2/SO. To test
199 whether actin oscillates during vegetative growth, germinated spores of wild-type LifeAct-GFP
200 were observed under the fluorescence microscope, in single cells with no interacting partner
201 nearby, and no oscillation was reported (Fig. 2C), indicating that oscillatory accumulation of
202 actin is exclusive to cell fusion growth.

203 ***Inhibition of MAK-2 disrupts the cell fusion process***

204 Based on previous results, it was hypothesized that MAK-1 may directly participate in actin
205 polymerization or that actin misregulation may be an indirect effect of the disruption of the cell
206 fusion process caused by MAK-1 inhibition. To test this hypothesis, a similar strategy was
207 followed by creating an analog-sensitive version of MAK-2 to decipher SO and actin dynamics
208 during the tropic growth phase. The generated MAK-2^{Q100A} (*Pmak-2-mak-2::Ptef-1-mak-*
209 *2^{Q100A}-hph*) strains exhibited a macroscopic phenotype similar to wild type in the presence of
210 DMSO and a Δ*mak-2*-like phenotype when the kinase was inhibited (Fig. S4A-C).
211 Microscopically, cell fusion rates were not fully comparable to the wild-type strain in the
212 presence of DMSO (73.8% vs 51.3%; WT/MAK-2^{Q100A}), but cell fusion was still observed. In
213 contrast, the cell fusion rate was comparable to Δ*mak-2* when the kinase inhibitor was added
214 (Fig. S4D). These data indicate that the strain is functional for cell fusion in the absence of the

215 kinase inhibitor and allow us to analyze the cell dynamics when MAK-2^{Q100A} is inhibited in a
216 spatial-temporal manner.

217 To evaluate the impact of MAK-2^{Q100A} inhibition on the subcellular localization of SO and actin,
218 we generated strains MAK-2^{Q100A} + SO-GFP and MAK-2^{Q100A} + LifeAct-GFP. We observed
219 that in the presence of DMSO, the dynamic localization of SO was similar to the wild-type
220 phenotype (Fig. 3A). However, upon addition of the kinase inhibitor, the oscillation of SO
221 rapidly ceased (within 4 minutes), and in 10 out of 15 observations, the localization of SO
222 remained broadly distributed around the cell membrane (Fig. S5A). Interestingly, in 5 out of
223 15 observations, the localization of SO shifted to a different area of the cell, suggesting that
224 the complex formed at the cell tips may travel together around the cell membrane after MAK-
225 2 inhibition (Fig. 3B). We also examined the localization of actin and observed fusing cell pairs
226 under the microscope in the presence of DMSO, displaying the previously described
227 oscillatory accumulation of actin at the cell tips (Fig. 3C). However, in the presence of the
228 kinase inhibitor, the actin localization shifted to a different position within the cell, with 10 out
229 of 20 observations displaying actin travelling to the opposite cell tip in a manner similar to that
230 of SO (Fig. 3B). After 10 minutes, actin still accumulated at the new position, despite the
231 termination of tropic interaction and directed growth (Fig. 3D). In some cases (10 out of 20),
232 actin shifted to a different position but remained close to the cell tip (Fig. S5B). These data
233 suggest that MAK-2 inhibition has a slightly different impact on the disruption of actin
234 localization and indicate that MAK-1 and MAK-2 may have distinct roles in cytoskeleton
235 organization during cell fusion. Moreover, the observed effect on actin localization rules out
236 the hypothesis of an indirect effect on actin cytoskeleton due to the disruption of cell fusion.

237 ***The actin cytoskeleton plays a crucial role in the dynamic localization of MAK-2 and SO***

238 The inhibition of MAK-1^{E104G} disrupts proper membrane recruitment of MAK-2/SO, while also
239 disturbing actin accumulation at the cell tips. Actin cables serve as tracks for the transport of
240 multiple cargoes, including potential secretory vesicles that may be involved in the cell fusion
241 process [18, 28]. Our data support two alternative hypotheses: either MAK-1 activity is directly
242 involved in both MAK-2/SO recruitment and actin organization, or it is only involved in actin
243 organization, and actin disruption results in disturbed MAK-2/SO localization.

244 In yeast, Fus3p recruitment is mainly mediated through actin cables organized at the Shmoo
245 of the mating cells [29]. To test whether actin is required for proper MAK-2/SO recruitment,
246 we employed the actin-disrupting drug latrunculin A [30]. In a pretest, we determined that a
247 concentration of 10 μM resulted in the dissociation of F-actin in germinating spores within 6-
248 10 minutes (Fig. S5C). When we tested MAK-2 localization, we observed that actin disruption
249 due to latrunculin A resulted in the disassembly of MAK-2 after 8 minutes, and no further MAK-

250 2 membrane recruitment was observed in the cells (Fig. 4A). Similarly, the dynamic
251 localization and membrane recruitment of SO were also affected by actin inhibition (Fig. 4B),
252 suggesting that proper actin polymerization at the cell tips is essential for membrane
253 recruitment of MAK-2 and SO. To further understand the implications of MAK-1/MAK-2 in this
254 process, we decided to investigate the roles of the upstream regulators of actin polymerization,
255 the Rho-GTPases.

256 Rho GTPases are conserved eukaryotic proteins that regulate actin dynamics by cycling
257 between active (GTP-bound) and inactive (GDP-bound) states [3]. Upon activation, they
258 translocate to the plasma membrane and interact with actin regulators, such as formins, to
259 promote actin cable formation. In filamentous fungi, RAC-1 and CDC-42 localize to growing
260 tips but play distinct roles in cell fusion and germ tube growth, respectively [19]. The RAC-1–
261 specific inhibitor NSC3766 has been used to distinguish their functions. In our experiments,
262 we tested if specific inhibition of RAC-1 with NSC3766 affects the dynamics of actin and the
263 recruitment of MAK-2, SO, and actin assembly. In interacting cell pairs expressing MAK-2-
264 GFP, the protein was recruited to the membrane in a wild-type manner before addition of RAC-
265 1 inhibitor. The addition of the RAC-1 inhibitor at a concentration of 100 μM resulted in defects
266 in the recruitment of MAK-2 after 12 minutes. MAK-2 fully disappeared from the membranes
267 of both cells and the interaction ended (Fig. 4C). When SO dynamics were tested, the usual
268 membrane accumulation at the cell tips was observed. Like the previous experiment, defects
269 in the localization of SO were observed 12 minutes after the addition of the RAC-1 inhibitor.
270 However, in contrast to MAK-2, SO remained widely distributed at the membranes of both
271 cells although the interaction had ended (Fig. 4D). To note, this mislocalization of SO was
272 comparable to the one observed after MAK-1 inhibition (actin patches distributed all around
273 the cell membrane), suggesting that both proteins (MAK-1 & RAC-1) may play functions within
274 the same pathway. We also examined actin localization in the presence of the RAC-1 inhibitor.
275 The addition of the inhibitor resulted in a decline in the number of actin cables, and actin
276 patches seems to be distributed more widely around the plasma membrane. After 12 minutes,
277 actin cables had fully disappeared and directed cell growth was terminated (Fig. S5D).

278 These data indicate that the proper polymerization of actin at the cell tips of the interacting
279 cells, through activation of the Rho GTPase RAC-1, is essential for the dynamic localization
280 of MAK-2 and SO.

281 ***MAK-1 activity is required for RAC-1 activation, whereas MAK-2 activity determines its***
282 ***positioning.***

283 Previously, we described a potential connection between the activity of MAK-1 and RAC-1.
284 Both proteins are necessary for actin assembly during cell fusion, and similar defects are

285 observed when each one is inhibited. In contrast, MAK-2 inhibition disrupts the cell
286 communication process, although the actin complex becomes unstable within the cell.
287 Together, these data support two potential hypotheses: MAK-1 and RAC-1 function in the
288 same pathway, either upstream or downstream, controlling actin polymerization, or RAC-1
289 and MAK-1 regulate, independently, a common target that is essential for actin assembly,
290 such as the formin BNI-1. To test these hypotheses, we decided to analyze the dynamics of
291 active RAC-1 after MAK-1 and MAK-2 inhibition using the Cdc42-Rac-interacting-binding
292 (CRIB) reporter. If the first hypothesis is correct, MAK-1 inhibition will inactivate RAC-1,
293 causing reporter detachment from the membrane. Since Rho GTPases associate with
294 membranes only when active, detachment indicates inactivation. Alternatively, if the second
295 hypothesis is correct, MAK-1 inhibition will not affect RAC-1, and the reporter will remain at
296 the plasma membrane, suggesting that MAK-1 and RAC-1 act independently on a common
297 factor involved in actin polymerization during cell fusion.

298 To note CRIB reporters in filamentous fungi binds as a GEF protein to activated Rho-GTPases
299 without disrupting their function, thereby allowing the localization of both activated RAC-1 and
300 CDC-42 at the same time in our fungal system [19]. The use of the highly specific RAC-1
301 inhibitor allowed to distinguish the functions of both proteins, since CDC-42 is unaltered by
302 this chemical. As a control, we first tested the already reported effects of RAC-1 inhibition on
303 the CRIB reporter. As previously described, the addition of the RAC-1 inhibitor to interacting
304 cells resulted in the disappearance of the reporter from the apical tip and cell growth arrest
305 (Fig. S6A). The complete disappearance of the reporter from the tips of the interacting cells
306 indicates that only RAC-1, and not CDC-42, is present at the growth cone of the fusing cells
307 [19].

308 In our study, we observed that the CRIB reporter was present permanently in both cell tips
309 during fusion, as previously shown [19] (Fig. 5A). Interestingly, following inhibition of MAK-1,
310 the CRIB reporter disappeared from the plasma membrane and cell growth was arrested (Fig.
311 5B). It is noteworthy that both RAC-1 and MAK-1 inhibition produced a similar effect on the
312 CRIB reporters, suggesting that MAK-1 inhibition specifically affects RAC-1 activity, leading to
313 the disruption of the actin assembly, membrane recruitment of MAK-2 and SO, and the general
314 fusion process. Consistent with our hypothesis, we predict that MAK-2 inhibition does not
315 affect the activity of RAC-1 but rather its localization, as previously observed with the actin in
316 earlier experiments. As previously observed, the localization of the CRIB reporter remained
317 permanently at both cell tips during the entire tropic growth phase in our control (Fig. 5C).
318 However, when MAK-2 was inhibited, the CRIB reporter remained recruited to the plasma
319 membrane, and its localization appeared to be widely distributed around the cell tip (Fig. 5D).

320 These suggest that MAK-2 may control the localization and, therefore, growth directionality of
321 RAC-1.

322 Nevertheless, as we have previously mentioned, the CRIB reporter allows for the localization
323 of the activated forms of both RAC-1 and CDC-42 at the same time. To determine if RAC-1,
324 and not CDC-42, changes its position after MAK-2 inhibition, we applied the RAC-1 inhibitor
325 after inhibiting MAK-2, combining both chemicals in a temporal resolution. Fusing cells were
326 observed under the microscope, and the kinase inhibitor was added. After observing the
327 switching in the position of the CRIB reporter provoked by MAK-2 inhibition, the RAC-1
328 inhibitor was added. Interestingly, the CRIB reporter disappeared completely from the plasma
329 membrane, indicating that MAK-2 inhibition of fusing cells affects exclusively the position of
330 RAC-1 at the plasma membrane (Fig. 5E & S6B). These data indicate that MAK-2 inhibition
331 in tropically growing cells specifically affects the localization of RAC-1, which remains active
332 and recruited to the plasma membrane but loses its growth directionality towards the cell
333 fusion partner and changes its position to another area in the cell.

334 Taken together, all these data support a model in which the inhibition of MAK-1 specifically
335 affects RAC-1 membrane recruitment, which results in the disassembly of the actin focus
336 organized by the Rho-GTPase and the arrest of growth of the interacting cells.

337 ***MAK-1 is a specific regulator of actin polymerization during cell fusion***

338 We have shown that MAK-1 activity is crucial for proper actin polymerization at the tips of
339 interacting cells during cell fusion. This leads to the question of whether MAK-1 functions
340 specifically in directed growth or whether it plays a role in general polar growth. To address
341 this question, we conducted an experiment to observe the effect of kinase and RAC-1
342 inhibitors (as a negative control) independently on non-interacting cells. The length of the germ
343 tube was quantified under a microscope before and after incubation with the kinase inhibitor,
344 RAC-1 inhibitor, or DMSO. To ensure that only non-interacting cells were tested, we analyzed
345 germlings that were at a distance of more than 30 µm from the nearest cell. Our results indicate
346 that there were no significant differences observed between the DMSO, kinase inhibitor, or
347 RAC-1 inhibitor treatments, supporting the notion that MAK-1/RAC-1 exclusively regulates
348 actin polymerization and therefore tropic growth during cell fusion (Fig. 6A). Additionally, we
349 conducted a similar experiment to test whether MAK-2 had any effect on growth rate and
350 obtained similar results (Fig. 6A).

351 Furthermore, we investigated the localization of the CRIB reporter and actin before and after
352 treatment with DMSO, kinase inhibitor, or RAC-1 inhibitor, in non-interacting cells. As
353 expected, there were no consistent differences observed in the localization of the CRIB
354 reporter when cells were treated with DMSO or the kinase inhibitor (Fig. 6B) and with H_2O (the

355 solvent for the RAC-1 inhibitor) or the RAC-1 inhibitor (Fig. 6C) in the MAK-1-inhibitable
356 strains. Similarly, no significant differences were observed in the localization of the CRIB
357 reporter when the cells were incubated with DMSO or the kinase inhibitor (Fig. 6B), H_2O, or
358 the RAC-1 inhibitor (Fig. 6C) in the MAK-1^{E104G} and MAK-2^{Q100A} (Fig. 6D and E).

359 To further confirm these findings from the chemical genetics approach, we studied actin
360 organization in the *mak-1* knockout mutant obtained from the *N. crassa* gene knockout
361 collection (NCU09482). A Δ*mak-1* LifeAct-GFP strain was created through sexual crosses
362 (see Materials and methods for more details). As previously reported, this mutant exhibited a
363 cell fusion-deficient phenotype [23]. The spores of this isolate were incubated in MM for 2
364 hours, and actin organization was studied using fluorescence microscopy. In the Δ*mak-1*
365 mutant cells, germ tube elongation and actin assembly at the growing cell tips were
366 comparable to wild type [18] (Fig. S6C).

367 Taken together, these data indicate that MAK-1 exclusively functions as an actin
368 polymerization regulator during the cell fusion process and is not involved in actin
369 polymerization during general vegetative growth. In other words, MAK-1 is not involved in the
370 same actin-regulatory pathway as CDC-42.

371 ***MAK-1 functions upstream of RAC-1***

372 MAK-1 has been identified as a key factor in regulating the communication and growth arrest
373 phases during cell fusion. This kinase plays a crucial role in the growth arrest phase, which
374 involves remodeling of the cell wall to allow for the completion of the fusion process. Analog-
375 sensitive versions of MAK-1 have been shown to partially inhibit the growth arrest phase,
376 resulting in disrupted cell merger and the emergence of a corkscrew-like phenotype in fusing
377 cells, also known as twisting germ tubes [20].

378 To investigate whether MAK-1 and RAC-1 are part of the same pathway, we conducted
379 experiments using wild-type cells and partial inhibition of RAC-1. We tested three different
380 concentrations of RAC-1 inhibitor (100, 50, and 25 μM), with only the latter concentration
381 allowing for the induction of cell fusion events (Fig. 7A). Furthermore, a large number of cells
382 exhibited defects in polar growth, which may be related to the effect of RAC-1 inhibition. To
383 further investigate this observation, we quantified the percentage of cells that showed tropic
384 defects (observed as growth-forming circles) after RAC-1 inhibition in medium with Ca^{2+}.
385 Approximately 12.5% of cells exhibited this growth, compared to the water control. To
386 determine whether this defect was caused by inhibition of the general germ tube elongation
387 machinery, we performed similar quantifications on wild-type cells placed on media without
388 Ca^{2+} (which inhibits the induction of cell fusion) and on a cell fusion mutant, such as Δ*so*. We

389 observed that polarity defects were not observed in either case, suggesting that this phenotype
390 may be caused by partial inhibition of RAC-1 specifically when cells are undergoing cell fusion
391 (Fig. 7B). Although MAK-1 and RAC-1 function within the same actin-regulatory pathway
392 during cell fusion, there is currently a lack of strong evidence to determine which protein is
393 upstream/downstream. Interestingly, both proteins are localized at the cell tips during the cell
394 growth arrest phase [19, 20]. Therefore, we conducted experiments to investigate how the
395 localization of MAK-1 and RAC-1 were affected after inhibition of RAC-1 or MAK-1, when the
396 cells are merging. To observe the effects of the subcellular localization of MAK-1/RAC-1, cells
397 that had just established contact were observed under a microscope and either RAC-1 or the
398 kinase inhibitor was added. When RAC-1 was observed, its localization remained at the
399 contact area of the fusing cells that had just made contact, and the addition of DMSO had no
400 effect on its localization (Fig. 8A). However, the complete inhibition of MAK-1 in fusing cells
401 rapidly induced mislocalization of RAC-1, which completely disappeared from the plasma
402 membrane while cells likely stopped their cellular interaction (Fig. 8B). The addition of water,
403 the solvent of the RAC-1 inhibitor, did not affect the cell fusion event and MAK-1 localization
404 during the final stages of cell fusion (Fig. 8C). Interestingly, the addition of the RAC-1 inhibitor
405 in interacting cells did not have any significant effect on the localization of MAK-1, which
406 remained at the contact area, although cells likely stopped their interaction (Fig. 8D).

407 These data indicate that the MAPK MAK-1 controls, and is therefore upstream of, the
408 activation and membrane-recruitment of RAC-1 during the cell fusion process.

409 ***Discussion***

410 Cell fusion in filamentous fungi is a minimalist paradigm of morphogenesis and cell
411 communication: genetically identical cells that nevertheless rely on several pathways to
412 convert a shared signal into a directed actin-based growth in an oscillatory manner. In this
413 study we show that the CWI MAPK MAK-1 is essential for activating the Rho GTPase RAC-1
414 and assembling the actin aster required for chemotropic growth, whereas the MAPK MAK-2
415 governs the spatial positioning of this RAC-1/Actin cluster. When MAK-1 activity is inhibited,
416 we observed that the actin cluster associated to the tips completely disappeared, arresting the
417 growth of the interacting cells (Fig. 9). Neurospora encodes six Rho-family GTPases, yet only
418 two, RAC-1 and CDC-42, direct polarized growth at the hyphal tip: RAC-1 drives the
419 specialized, chemotropic growth that ends in cell fusion, whereas CDC-42 handles vegetative
420 extension. Our observations match what Lichius *et al*. reported: when RAC-1 is blocked with
421 NSC23766, the RAC-1-active CRIB reporter vanishes, the actin focus dissolves, and growth
422 is arrested, while CDC-42 is unaffected and keeps normal chemotropic growth running [19].
423 We see the same split, RAC-1 inhibition recreates the MAK-1-block phenotype, but CDC-42

424 activity and the actin cap at non-interacting tips stay intact, confirming that MAK-1 channels
425 its fusion-specific actin signal through RAC-1 rather than CDC-42. Neurospora carries a single
426 formin, BNI-1, which, like most formins, is normally activated when a GTP-loaded Rho protein
427 binds its regulatory domain, releasing autoinhibition and enabling actin-cable assembly [31].
428 Surprisingly, however, *bni-1*Δ germlings still undergo fusion and even display a "hyper-fusion"
429 phenotype in which peripheral tips fuse [32]. These observations argue that BNI-1 is not the
430 principal or sole organizer of the fusion actin focus. MAK-1 might therefore influence actin in
431 two, non-exclusive ways: (i) indirectly, by activating RAC-1, which in turn could stimulate BNI-
432 1 activity; or (ii) directly, by phosphorylating BNI-1 (or an alternative actin nucleator) and
433 thereby modulating actin assembly independently of RAC-1. Precedents for both routes exist
434 in higher eukaryotes. The canonical MAPK ERK1/2 phosphorylates the Rho-GEF GEF-H1 to
435 activate the Rho GTPase RhoA [33], while ERK3 not only serves as a GEF for CDC-42/RAC-
436 1 but also phosphorylates the Arp3 subunit of the Arp2/3 complex, boosting actin
437 polymerization. The Arp2/3 complex is the principal catalyst of branched-actin assembly,
438 converting linear filaments into meshworks. In Neurospora, deletion of any Arp2/3 subunit
439 reduces cell-fusion frequency by ~2.5-fold yet leaves germination unaffected [25], suggesting
440 that Arp2/3, like RAC-1, plays a fusion-specific role and could lie downstream of MAK-1.
441 Arp2/3 may work together with BNI-1 or compensate for it when BNI-1 is absent (in *bni-1*Δ)
442 during fusion. Defining how these nucleators fit into the MAK-1 pathway remains an open
443 question.

444 Importantly, no evidence currently links CWI MAPKs to direct phosphorylation of RAC
445 proteins. A phosphoproteomic assay of the *Aspergillus fumigatus* CWI MAPK MpkA (the
446 MAK-1 orthologue) catalogued hundreds of MpkA-dependent phosphosites [34];
447 Supplementary Table S1A) yet did not list the AfRAC-1 (UniProt Q4WWL5) among the
448 modified targets, reinforcing the notion that RAC-type GTPases are controlled indirectly rather
449 than being direct MAPK substrates. Our own data support this view. Inhibiting MAK-1 causes
450 the CRIB-GFP reporter to detach from the plasma membrane, mirroring the loss of RAC-1
451 signal seen when RAC-1 is chemically blocked with NSC23766 (Fig S6A) [32]. Membrane
452 detachment is diagnostic of RAC-1 inactivation, indicating that MAK-1 activity is required to
453 keep RAC-1 in its GTP-bound state, most plausibly via phosphorylation of an upstream
454 activator. By contrast, inhibiting MAK-2 stops the interaction but leaves RAC-1 on the
455 membrane; the reporter simply relocates to ectopic cortical sites, underscoring MAK-2 role in
456 positioning rather than activating the GTPase. Collectively, these observations favor a model
457 in which MAK-1 sustains RAC-1 activity likely through a yet-to-be-identified GEF or scaffold,
458 while MAK-2 provides the spatial cue that keeps the active RAC-1/actin complex aimed at the
459 fusion partner. A striking parallel comes from the Neurospora ergosterol biosynthesis mutant

460 *erg-2*Δ; perturbing ergosterol composition destabilizes sterol-rich membrane domains (SRDs)
461 at the cell tip and produces the same twisting germ-tube phenotype seen under partial MAK-
462 1 or RAC-1 inhibition (Fig. 7A and B), whereas MAK-2 inhibition simply arrest growth without
463 twisting [20]. SRDs are recognized polarity platforms in several systems: loss of tip-associated
464 SRDs in *Aspergillus fumigatus* or yeast prevent recruitment of polarity organizers and results
465 in growth inhibition [35, 36]. In mammalian cells, Rac1 activation itself requires intact lipid rafts
466 [37]. The matching phenotypes caused by *erg-2*Δ, partial RAC-1 inhibition, and partial MAK-
467 1 inhibition therefore support a model in which SRDs maintain RAC-1 in its active, tip-localised
468 state, most likely via a MAK-1-dependent GEF. Compromising either the SRD scaffold or
469 MAK-1/RAC-1 activity allows RAC-1 to drift from the apex, producing the characteristic twisted
470 morphology seen in *erg-2*Δ germ tubes. This also suggest that inhibition of MAK-2 may scatter
471 the sterol-rich tip patch itself: as the patch drifts around the membrane cortex, it drags the
472 RAC-1/actin complex with it, losing their fixed direction, potentially due to a loss of phase-
473 separation at the cell tips [38], an idea we revisit in the next paragraphs. Previous studies
474 made the hierarchy of the cytoskeleton clear in Neurospora: benomyl-induced loss of
475 microtubules leaves chemotropic interaction unaltered, whereas latrunculin B mediated
476 depolymerization of actin stops tip extension and abolishes fusion [25]. Consistent with this
477 actin dependence, we now see that actin intensity at the two fusion tips oscillates out of phase
478 with the MAK-2/SO signal: actin oscillates independently whether SO or MAK-2 is associated
479 to the tip of the interacting cell. The oscillatory cell dialog has also been described in the
480 nematode-trapping fungus *Arthrobotrys flagrans* [39], but the pattern there is markedly
481 different. In single Arthrobotrys hyphae, in non-interacting cells (described by the authors as
482 a monologue), actin, the SO homologue SofT and the MAK-2 homologue MakB all rise and
483 fall in synchrony, paced by an intrinsic growth oscillator. Only when two hyphae approach do
484 those in-phase oscillations slow, entrain and eventually split into the familiar anti-phasic
485 dialogue between partners [39]. By contrast, *Neurospora* shows no sign of a pre-existing
486 growth oscillator; its actin remains strictly anti-phasic to MAK-2/SO and the rhythm emerges
487 exclusively during cell-to-cell communication. These contrasts imply that the temporal
488 coupling between signaling, and actin assembly has diverged in the two lineages, so insights
489 from Arthrobotrys should be extrapolated to Neurospora with appropriate interpretation.

490 Mating of the fission yeast *Schizosaccharomyces pombe* offers a well-resolved template for
491 how an actin focus can be integrated with MAPK signaling during fusion. Studies showed that
492 the formin Fus1 nucleates a compact, aster-like actin array, the fusion focus, exactly at the
493 contact site between the two cells [28]. Super-resolution imaging and live secretion assays
494 revealed that this aster acts as a “cargo concentrator,” corralling vesicles laden with cell wall
495 hydrolases so that enzymatic thinning, membrane juxtaposition, and actin-driven force are

496 synchronized. The focus also hosts the pheromone MAPK cascade (MAPK Spk1 and its
497 upstream tiers), creating a signaling hot-spot that locks the cells into the fusion programme.
498 A key mechanistic insight is that the intrinsically disordered region (IDR) of Fus1 undergoes
499 liquid–liquid phase separation: the IDR self-associates to form a condensate whose network
500 simultaneously traps actin regulators, vesicle tethers, and MAPK components in a nanometer-
501 scale volume, greatly boosting their local concentration and reaction rates [38]. Our
502 Neurospora data point to a conceptually similar, though compositionally distinct, hub. The
503 formin BNI-1 is dispensable for the fusion aster, yet two scaffold proteins, HAM-5 and, critically
504 SO, co-localize with the RAC-1/actin complex at the tip. SO is already known to anchor the
505 entire three-tier CWI cascade (including MAK-1) [40], but only SO, not MAK-1, participates in
506 the cell dialog oscillatory dynamic localization, implying that SO fulfils additional, MAPK-
507 independent roles. We therefore propose that MAK-2 (and the signaling cargo it guides) is
508 delivered into a HAM-5 condensate at the apex, where high local concentration of RAC-1 and
509 actin nucleators enforces directionality, in association with SRDs. Whether SO or HAM-5 truly
510 phase-separate, and how MAK-2 activity is choreographed within such a compartment,
511 remains an open question.

512 Taken together, these oscillation patterns point to species-specific timing circuits that are
513 governed by the upstream MAPKs MAK-1 and MAK-2. Based on our findings we propose a
514 model in which MAK-1 initiates fusion by potentially activating RAC-1 (or perhaps another,
515 yet-unknown actin nucleator) to build the actin aster, whereas MAK-2 continually reorients that
516 aster toward the opposite cell tip (Fig. 9). This system has some similarities with the situation
517 in budding-yeast mating, where the pheromone-response MAPK Fus3 (homolog to MAK-2)
518 redirects growth toward the other partner [41]. Unlike yeast mating, Neurospora somatic cell
519 fusion is pheromone-independent, and its ligand-receptor pair remains unidentified, yet in both
520 systems a dedicated MAPK module converts an external cue into precise spatial guidance of
521 the polarity machinery.

522 Material and methods

523 *N. crassa strains and media*

524 The strains generated and used in this study are listed in the supplementary information (Table
525 S1). Strains were generally grown in Vogel's Minimal Medium (VMM) (Vogel, 1956)
526 supplemented with 2% sucrose as the carbon source and with 1.5% agar for solid media.
527 Generally, all strains were incubated in solid VMM (supplemented with histidine 0.5 mg/ml
528 when needed) for 3-4 days in dark at 30ºC and an additional day with natural light at room
529 temperature. Homokariotic strains were purified by either single spore isolation (SSPi) or by
530 crossing with the wild-type strain. For selection during SSPi, VMM with hygromycin was

531 employed. Crosses were performed on Westergaard's medium as described earlier
532 (Westergaard and Mitchell, 1947). The ascospores obtained from the crosses were
533 germinated in VMM with hygromycin and confirmed by polymerase chain reaction (PCR).

534 *Plasmid construction*

535 The primers used for the generation of the plasmids are listed in table S2. In order to construct
536 the *mak-1*^{E104G} (analog-sensitive) knock-in cassette, a fragment containing a 5´ upstream
537 region together with the *mak-1* open reading frame was PCR-amplified using the primers 1304
538 and 1305 and using the previously generated *mak-1*^{E104G}*-gfp* plasmid as a template (Weichert
539 et al., 2016). By yeast recombinational cloning, the resulting fragment was fused to the
540 hygromycin resistance cassette (amplified with primers 82 and 83) and a 1 kb fragment
541 homologous to the 3' downstream region of *mak-1* (generated with primers 1306 and 1307),
542 resulting in the plasmid 738.

543 For the generation of the *Ptef-1-mak-2*^{Q100A} strain, the fragments required for the construction
544 of the gene knock-in cassette were amplified by PCR. A 1 kb genomic region positioned 2 kb
545 upstream of the *mak-2* promoter (considering it to be the 1 kb region upstream of the coding
546 read frame) was amplified with primers 1489 and 1490. The *Ptef-1-mak-2*^{Q100A}*-gfp* plasmid
547 used in a previous study [24] served as a template for the amplification of the *Ptef-1-mak-*
548 *2*^{Q100A} PCR fragment with primers 1488 and 1487. The resistance cassette used was *Hyg*^{R},
549 which was amplified with primers 82 and 83. Finally, the 1 kb genomic region downstream of
550 the *mak-2* Stop-codon was amplified with primers 1489 and 1492. The four fragments were
551 fused by yeast recombinational cloning generating the plasmid 846. The plasmid 723 (*Ptef-1-*
552 *dsRed-so*) was generated by cloning of the *so* ORF amplified with primers 1419 and 1420 and
553 ligated into the plasmid 722 (pMF334-Tef-dsRed) with enzymes AscI/XbaI. The resulting
554 plasmid was transformed into N1-03 generating the strain 843 (*his-3::Ptef-1-dsRed-so*). Yeast
555 recombinational cloning was performed as previously described (Da et al., 2000).

556 *Strain generation*

557 All strains were either generated by transformation as described in early studies (Margolin et
558 al., 1997) or by crossing (Westergaard and Mitchell, 1947). When indicated, strains were
559 purchased to the Fungal Genetics Stock Center. A helpful list of protocols and media
560 description is available at their website (www.fgsc.net).

561 For generating the inhibitable MAK-1 strain, the gatekeeper amino acid, glutamine at position
562 104, was exchanged with glycine to render the kinase analog-sensitive, resulting in the *mak-*
563 *1*^{E104G} gene [20]. The plasmid 738 containing the *mak-1*^{E104G}*-hph* construct was used as a

564 template to amplify the full-length knock-in fragment by PCR (using primers 1304 and 1307),
565 which was then transformed into the *N. crassa* strain N1-06 (FGSC 9719) (Fig. S1A). This
566 recipient strain has a mutation in the gene *mus52*, which increases the frequency of
567 homologous recombination up to almost 100% [42]. The resulting transformants were first
568 tested by PCR to confirm the base pair exchange (E104G; CAG to GGC), and the proper
569 integration of the transforming DNA was confirmed by Southern blot of homokaryotic isolates
570 obtained from a sexual cross of the primary transformants with the wild-type strain (Fig. S1A
571 and B). To generate the subsequent strains combining reporters and MAK-1^{E104G}, strain 849,
572 carrying the *mak-1::mak-1^{E104G}-hph* genotype, was crossed independently with strains 665
573 and 714, which carried the *his-3::Ptef-1-mak-2-gfp* and *his-3::Ptef-1-so-gfp* constructs,
574 respectively, resulting in strains 865 and 874. The integration of the *mak-1::mak-1^{E104G}-hph*
575 locus and GFP constructs was confirmed by PCR and fluorescence microscopy, respectively.
576 For LifeAct, strain 849 was crossed with 754 (*his-3::Ptef-1-lifeact-gfp*), resulting in strain 869.
577 The CLA-4 CRIB reporter strain (*Pccg1::crib^cla-4-gfp::bar*+, 927) was crossed with the MAK-
578 1^{E104G} strain (849), resulting in strain 943 (*mak-1::mak-1^{E104G}-hph; Pal1-crib^cla-4-bar*).
579 Progenies were tested by fluorescence microscopy and PCR.

580 Analogous to the design of the *mak-1^{E104G}-hph* construct, a *mak-2^{Q100A}-hph* gene knock-in
581 cassette was created and integrated at the original gene locus of strain N1-06 (Δ*mus-52*).
582 However, this construct was found to be non-functional, and the respective transformants
583 exhibited a Δ*mak-2*-like phenotype (data not shown). In previous work at our laboratory, we
584 found that the Δ*mak-2* phenotype of the knock-out mutant was only fully complemented when
585 the WT or the analog-sensitive version was overexpressed using strong constitutive promoters
586 such as P*ccg-1* or P*tef-1* [8, 24]. Therefore, the promoter at the original gene locus was
587 replaced by the P*tef-1* sequence. The linear *Ptef-1-mak-2^{Q100A}-hph* knock-in cassette,
588 amplified from the plasmid 846 with primers 1487 and 1488, was transformed into N1-05
589 (Δ*mus-52*, like N1-06 but different mating type), resulting in strain 882 (*Pmak-2-mak-2::Ptef-*
590 *1-mak-2^{Q100A}-hph*). The primary transformants were tested by PCR of the *mak-2* locus and
591 sequencing of the resulting fragment. To obtain a homokaryotic strain, a sexual cross was
592 performed between wild type mat a (N1-02) and one of the primary transformants, 882 (mat
593 A). Four of the resulting progenies were tested by Southern blot analysis for single integration
594 of the construct. All four isolates showed clear bands corresponding to the *Ptef-1-mak-2^{Q100A}*
595 radioactive-labelled fragment, while it was absent in the recipient strain (N1-05) (Fig. S4A and
596 B). To generate the subsequent strains combining reporters and MAK-2^{Q100A}, we performed a
597 genetic cross between the strain *Pmak-2-mak-2::Ptef-1-mak-2^{Q100A}-hph* (899) and two
598 additional strains, 714 (*his-3::Ptef-1-so-gfp*) and 754 (*his-3::Ptef-1-lifeact-gfp*). This generated
599 two new strains: *his-3::Ptef-1-so-gfp; Pmak-2-mak-2::Ptef-1-mak-2^{Q100A}-hph* (912) and *his-*

600 *3::Ptef-1-lifeact-gfp; Pmak-2-mak-2::Ptef-1-mak-2^{Q100A}-hph* (915), respectively. The CRIB
601 reporter strain was generated by crosses of 927 (*Pal1-crib^cla-4-bar*) with MAK-2^{Q100A}; 899
602 (*Pmak-2-mak-2::Ptef-1-mak-2^{Q100}A-hph*), resulting in strain 949 (*Pmak-2-mak-2::Ptef-1-mak-*
603 *2^{Q100}A-hph;Pal1-crib^cla-4-bar*).

604 An actin-labeled Δ*mak-1* strain was obtained by setting up a sexual cross between the Δ*mak-*
605 *1* (NCU09482; purchased to the Fungal Genetics Stock Center; www.fgsc.net) and 754 (*his-*
606 *3::Ptef-1-lifeact-gfp*), resulting in the 891 strain (*mak-1::hph;his-3::Ptef-1-lifeact-gfp*).

607 *Live-cell imaging*

608 Sample preparation was performed as previously described (Schürg et al., 2012). For
609 observation of hyphal fusion in *N. crassa*, 5 µl of a 10^7-spore suspension were inoculated on
610 the side of a MM agar plate and incubated for 15 hours at 30ºC. The preparation of the sample
611 was performed in a similar way than for the spores. The microscope used and the settings for
612 software analyses were described in an early study (Serrano et al., 2018). All fluorescence
613 images shown in this study were processed by the widely used commercial deconvolution
614 software Huygens (by Scientific Volume Imaging), more specifically the Huygens Essential
615 version. Z-stacks (usually n=10) up to 100 nm of all fluorescence images were captured and
616 assembled as a single tiff file by using ImageJ (image-stacks-image to stack). The composite
617 images were processed through the deconvolution software with the following parameters (40-
618 100 iterations, 12 signal/noise ratio and 0.01% of quality change thresh).

619 *Quantitative analyses*

620 Quantification of the cell fusion and germination rate was performed as described elsewhere
621 (Fleissner et al., 2009; Schürg et al., 2012). For all cell fusion quantifications at least 100
622 spores were quantified per sample/condition, and at least three independent repetitions were
623 studied.

624 *Chemical inhibition*

625 Three different chemicals were used for the corresponding experiments. Latrunculin A (10
626 µM), dissolved in water, was used to test the consequences of actin-polymerization inhibition,
627 1-NM-PP1 (40 µm) dissolved in DMSO was used to test the inhibition of the analog-sensitive
628 kinases, and NSC23766 (100 µM/25 µM), dissolved in water, was used for specific inhibition
629 of the Rho-GTPase RAC-1. As a control, either water or DMSO 1% was used. For all inhibitor
630 experiments, fresh spores were harvested and incubated for 2 hours at 30ºC in MM plates. A
631 1 cm^2 piece was cut from the agar plate and inverted onto a coverslip. The chemical was
632 added on the sample prior inversion onto the coverslip or on one side of the agar block.

633 *Statistics applied to the data*

634 All quantitative data were statistically analyzed by performing a two-tailed unpaired t-test using
635 Excel. The P values were calculated for 0.001, 0.05 or 0.01, and indicated as ***, ** or *
636 respectively. To analyze whether the variances were paired or unpaired, F-test analyses were
637 performed.

638 **References**

639 1. Bentley M, Banker G. The cellular mechanisms that maintain neuronal polarity.
640 Nature Reviews Neuroscience. 2016;17(10):611-22. doi: 10.1038/nrn.2016.100.
641 2. Cheung AY, Wu H-m. Structural and Signaling Networks for the Polar Cell Growth
642 Machinery in Pollen Tubes. Annual Review of Plant Biology. 2008;59(Volume 59, 2008):547-
643 72. doi: https://doi.org/10.1146/annurev.arplant.59.032607.092921.
644 3. Martin SG, Arkowitz RA. Cell polarization in budding and fission yeasts. FEMS
645 Microbiology Reviews. 2014;38(2):228-53. doi: 10.1111/1574-6976.12055.
646 4. Arkowitz RA, Bassilana M. Polarized growth in fungi: Symmetry breaking and hyphal
647 formation. Seminars in Cell & Developmental Biology. 2011;22(8):806-15. doi:
648 https://doi.org/10.1016/j.semcdb.2011.08.010.
649 5. Harris SD. Cell Polarity in Filamentous Fungi: Shaping the Mold. International
650 Review of Cytology. 251: Academic Press; 2006. p. 41-77.
651 6. Riquelme M, Aguirre J, Bartnicki-García S, Braus GH, Feldbrügge M, Fleig U, et al.
652 Fungal Morphogenesis, from the Polarized Growth of Hyphae to Complex Reproduction and
653 Infection Structures. Microbiol Mol Biol Rev. 2018;82(2). Epub 20180411. doi:
654 10.1128/mmbr.00068-17. PubMed PMID: 29643171; PubMed Central PMCID:
655 PMCPMC5968459.
656 7. Fischer MS, Glass NL. Communicate and Fuse: How Filamentous Fungi Establish
657 and Maintain an Interconnected Mycelial Network. Front Microbiol. 2019;10:619. Epub
658 20190329. doi: 10.3389/fmicb.2019.00619. PubMed PMID: 31001214; PubMed Central
659 PMCID: PMCPMC6455062.
660 8. Fleissner A, Leeder AC, Roca MG, Read ND, Glass NL. Oscillatory recruitment of
661 signaling proteins to cell tips promotes coordinated behavior during cell fusion. Proc Natl
662 Acad Sci U S A. 2009;106(46):19387-92. Epub 20091102. doi: 10.1073/pnas.0907039106.
663 PubMed PMID: 19884508; PubMed Central PMCID: PMCPMC2780775.
664 9. Serrano A, Hammadeh HH, Herzog S, Illgen J, Schumann MR, Weichert M, et al.
665 The dynamics of signal complex formation mediating germling fusion in *Neurospora crassa*.
666 Fungal Genet Biol. 2017;101:31-3. Epub 20170216. doi: 10.1016/j.fgb.2017.02.003. PubMed
667 PMID: 28216441.

668 10. Atay O, Skotheim JM. Spatial and temporal signal processing and decision making
669 by MAPK pathways. Journal of Cell Biology. 2017;216(2):317-30. doi:
670 10.1083/jcb.201609124.
671 11. Turrà D, Segorbe D, Di Pietro A. Protein Kinases in Plant-Pathogenic Fungi:
672 Conserved Regulators of Infection. Annual Review of Phytopathology. 2014;52(Volume 52,
673 2014):267-88. doi: https://doi.org/10.1146/annurev-phyto-102313-050143.
674 12. Levin DE. Cell wall integrity signaling in Saccharomyces cerevisiae. Microbiol Mol
675 Biol Rev. 2005;69(2):262-91. doi: 10.1128/mmbr.69.2.262-291.2005. PubMed PMID:
676 15944456; PubMed Central PMCID: PMCPMC1197416.
677 13. Mishra R, van Drogen F, Dechant R, Oh S, Jeon NL, Lee SS, et al. Protein kinase C
678 and calcineurin cooperatively mediate cell survival under compressive mechanical stress.
679 Proceedings of the National Academy of Sciences. 2017;114(51):13471-6. doi:
680 doi:10.1073/pnas.1709079114.
681 14. Sieber B, Coronas-Serna JM, Martin SG. A focus on yeast mating: From pheromone
682 signaling to cell-cell fusion. Semin Cell Dev Biol. 2023;133:83-95. Epub 20220209. doi:
683 10.1016/j.semcdb.2022.02.003. PubMed PMID: 35148940.
684 15. Cansado J, Soto T, Franco A, Vicente-Soler J, Madrid M. The Fission Yeast Cell
685 Integrity Pathway: A Functional Hub for Cell Survival upon Stress and Beyond. Journal of
686 Fungi. 2022;8(1):32. PubMed PMID: doi:10.3390/jof8010032.
687 16. Maddi A, Dettman A, Fu C, Seiler S, Free SJ. WSC-1 and HAM-7 are MAK-1 MAP
688 kinase pathway sensors required for cell wall integrity and hyphal fusion in *Neurospora*
689 *crassa*. PLoS One. 2012;7(8):e42374. Epub 20120803. doi: 10.1371/journal.pone.0042374.
690 PubMed PMID: 22879952; PubMed Central PMCID: PMCPMC3411791.
691 17. Pandey A, Roca MG, Read ND, Glass NL. Role of a mitogen-activated protein kinase
692 pathway during conidial germination and hyphal fusion in *Neurospora crassa*. Eukaryot Cell.
693 2004;3(2):348-58. doi: 10.1128/ec.3.2.348-358.2004. PubMed PMID: 15075265; PubMed
694 Central PMCID: PMCPMC387641.
695 18. Berepiki A, Lichius A, Shoji JY, Tilsner J, Read ND. F-actin dynamics in *Neurospora*
696 *crassa*. Eukaryot Cell. 2010;9(4):547-57. Epub 20100205. doi: 10.1128/ec.00253-09.
697 PubMed PMID: 20139238; PubMed Central PMCID: PMCPMC2863416.
698 19. Lichius A, Goryachev AB, Fricker MD, Obara B, Castro-Longoria E, Read ND. CDC-
699 42 and RAC-1 regulate opposite chemotropisms in *Neurospora crassa*. Journal of Cell
700 Science. 2014;127(9):1953-65. doi: 10.1242/jcs.141630.
701 20. Weichert M, Lichius A, Priegnitz B-E, Brandt U, Gottschalk J, Nawrath T, et al.
702 Accumulation of specific sterol precursors targets a MAP kinase cascade mediating cell–cell
703 recognition and fusion. Proceedings of the National Academy of Sciences.
704 2016;113(42):11877-82. doi: doi:10.1073/pnas.1610527113.

705 21. Bishop AC, Ubersax JA, Petsch DT, Matheos DP, Gray NS, Blethrow J, et al. A
706 chemical switch for inhibitor-sensitive alleles of any protein kinase. Nature.
707 2000;407(6802):395-401. doi: 10.1038/35030148. PubMed PMID: 11014197.
708 22. Fleißner A. Turning the switch: using chemical genetics to elucidate protein kinase
709 functions in filamentous fungi. Fungal Biology Reviews. 2013;27(1):25-31. doi:
710 https://doi.org/10.1016/j.fbr.2013.02.001.
711 23. Fu C, Iyer P, Herkal A, Abdullah J, Stout A, Free SJ. Identification and
712 characterization of genes required for cell-to-cell fusion in *Neurospora crassa*. Eukaryot Cell.
713 2011;10(8):1100-9. Epub 20110610. doi: 10.1128/ec.05003-11. PubMed PMID: 21666072;
714 PubMed Central PMCID: PMCPMC3165452.
715 24. Serrano A, Illgen J, Brandt U, Thieme N, Letz A, Lichius A, et al. Spatio-temporal
716 MAPK dynamics mediate cell behavior coordination during fungal somatic cell fusion.
717 Journal of Cell Science. 2018;131(9). doi: 10.1242/jcs.213462.
718 25. Roca MG, Kuo HC, Lichius A, Freitag M, Read ND. Nuclear dynamics, mitosis, and
719 the cytoskeleton during the early stages of colony initiation in *Neurospora crassa*. Eukaryot
720 Cell. 2010;9(8):1171-83. Epub 20100305. doi: 10.1128/ec.00329-09. PubMed PMID:
721 20207852; PubMed Central PMCID: PMCPMC2918927.
722 26. Fleißner A, Serrano A. 7 The Art of Networking: Vegetative Hyphal Fusion in
723 Filamentous Ascomycete Fungi. In: Wendland J, editor. Growth, Differentiation and
724 Sexuality. Cham: Springer International Publishing; 2016. p. 133-53.
725 27. Goryachev AB, Lichius A, Wright GD, Read ND. Excitable behavior can explain the
726 “ping-pong” mode of communication between cells using the same chemoattractant.
727 BioEssays. 2012;34(4):259-66. doi: https://doi.org/10.1002/bies.201100135.
728 28. Dudin O, Bendezú FO, Groux R, Laroche T, Seitz A, Martin SG. A formin-nucleated
729 actin aster concentrates cell wall hydrolases for cell fusion in fission yeast. J Cell Biol.
730 2015;208(7):897-911. doi: 10.1083/jcb.201411124. PubMed PMID: 25825517; PubMed
731 Central PMCID: PMCPMC4384723.
732 29. Qi M, Elion EA. Formin-induced actin cables are required for polarized recruitment of
733 the Ste5 scaffold and high level activation of MAPK Fus3. J Cell Sci. 2005;118(Pt 13):2837-
734 48. Epub 20050616. doi: 10.1242/jcs.02418. PubMed PMID: 15961405.
735 30. Coué M, Brenner SL, Spector I, Korn ED. Inhibition of actin polymerization by
736 latrunculin A. FEBS Lett. 1987;213(2):316-8. doi: 10.1016/0014-5793(87)81513-2. PubMed
737 PMID: 3556584.
738 31. Goode BL, Eck MJ. Mechanism and function of formins in the control of actin
739 assembly. Annu Rev Biochem. 2007;76:593-627. doi:
740 10.1146/annurev.biochem.75.103004.142647. PubMed PMID: 17373907.

741 32. Lichius A, Yáñez-Gutiérrez ME, Read ND, Castro-Longoria E. Comparative live-cell
742 imaging analyses of SPA-2, BUD-6 and BNI-1 in *Neurospora crassa* reveal novel features of
743 the filamentous fungal polarisome. PLoS One. 2012;7(1):e30372. Epub 20120124. doi:
744 10.1371/journal.pone.0030372. PubMed PMID: 22291944; PubMed Central PMCID:
745 PMCPMC3265482.
746 33. Fujishiro S-h, Tanimura S, Mure S, Kashimoto Y, Watanabe K, Kohno M. ERK1/2
747 phosphorylate GEF-H1 to enhance its guanine nucleotide exchange activity toward RhoA.
748 Biochemical and Biophysical Research Communications. 2008;368(1):162-7. doi:
749 https://doi.org/10.1016/j.bbrc.2008.01.066.
750 34. Mattos EC, Silva LP, Valero C, de Castro PA, Dos Reis TF, Ribeiro LFC, et al. The
751 *Aspergillus fumigatus* Phosphoproteome Reveals Roles of High-Osmolarity Glycerol
752 Mitogen-Activated Protein Kinases in Promoting Cell Wall Damage and Caspofungin
753 Tolerance. mBio. 2020;11(1). Epub 20200204. doi: 10.1128/mBio.02962-19. PubMed PMID:
754 32019798; PubMed Central PMCID: PMCPMC7002344.
755 35. Makushok T, Alves P, Huisman Stephen M, Kijowski Adam R, Brunner D. Sterol-Rich
756 Membrane Domains Define Fission Yeast Cell Polarity. Cell. 2016;165(5):1182-96. doi:
757 10.1016/j.cell.2016.04.037.
758 36. Takeshita N, Higashitsuji Y, Konzack S, Fischer R. Apical Sterol-rich Membranes Are
759 Essential for Localizing Cell End Markers That Determine Growth Directionality in the
760 Filamentous Fungus *Aspergillus nidulans*. Molecular Biology of the Cell. 2008;19(1):339-51.
761 doi: 10.1091/mbc.e07-06-0523. PubMed PMID: 18003978.
762 37. Fujitani M, Honda A, Hata K, Yamagishi S, Tohyama M, Yamashita T. Biological
763 activity of neurotrophins is dependent on recruitment of Rac1 to lipid rafts. Biochem Biophys
764 Res Commun. 2005;327(1):150-4. doi: 10.1016/j.bbrc.2004.11.151. PubMed PMID:
765 15629443.
766 38. Billault-Chaumartin I, Muriel O, Michon L, Martin SG. Condensation of the fusion
767 focus by the intrinsically disordered region of the formin Fus1 is essential for cell-cell fusion.
768 Curr Biol. 2022;32(21):4752-61.e10. Epub 20221005. doi: 10.1016/j.cub.2022.09.026.
769 PubMed PMID: 36202103; PubMed Central PMCID: PMCPMC9671092.
770 39. Wernet V, Kriegler M, Kumpost V, Mikut R, Hilbert L, Fischer R. Synchronization of
771 oscillatory growth prepares fungal hyphae for fusion. eLife. 2023;12:e83310. doi:
772 10.7554/eLife.83310.
773 40. Teichert I, Steffens EK, Schnaß N, Fränzel B, Krisp C, Wolters DA, et al. PRO40 is a
774 scaffold protein of the cell wall integrity pathway, linking the MAP kinase module to the
775 upstream activator protein kinase C. PLoS Genet. 2014;10(9):e1004582. Epub 20140904.
776 doi: 10.1371/journal.pgen.1004582. PubMed PMID: 25188365; PubMed Central PMCID:
777 PMCPMC4154660.

778 41. Yu RC, Pesce CG, Colman-Lerner A, Lok L, Pincus D, Serra E, et al. Negative
779 feedback that improves information transmission in yeast signalling. Nature.
780 2008;456(7223):755-61. doi: 10.1038/nature07513. PubMed PMID: 19079053; PubMed
781 Central PMCID: PMCPMC2716709.
782 42. Ninomiya Y, Suzuki K, Ishii C, Inoue H. Highly efficient gene replacements in
783 Neurospora strains deficient for nonhomologous end-joining. Proc Natl Acad Sci U S A.
784 2004;101(33):12248-53. Epub 20040806. doi: 10.1073/pnas.0402780101. PubMed PMID:
785 15299145; PubMed Central PMCID: PMCPMC514464.
786 43. Lichius A, Goryachev AB, Fricker MD, Obara B, Castro-Longoria E, Read. CDC-42
787 and RAC-1 Regulate Opposite Chemotropisms in *Neurospora Crassa*. Journal of cell
788 science. 2014;127(Pt 9). doi: 10.1242/jcs.141630. PubMed PMID: 24790223.

789 **Figures**

790 **Figure 1. Activity inhibition of MAK-1 disrupts the oscillatory localization of MAK-2/SO**
791 **and LifeAct**. **(A)** Oscillatory localization of MAK-2-GFP during cell fusion in a MAK-1^{E104G}
792 background (strain 865) with the addition of DMSO. **(B)** Inhibition of MAK-1^{E104G} disrupts the
793 oscillatory dynamic localization of MAK-2. **(C)** Oscillatory dynamic localization of SO during
794 cell fusion in a MAK-1^{E104G} background (strain 874) with the addition of DMSO. **(D)** Inhibition
795 of MAK-1^{E104G} disrupts the oscillatory dynamic localization of SO. **(E)** Oscillatory localization
796 of LifeAct-GFP during cell fusion in a MAK-1^{E104G} background (strain 869) with the addition
797 of DMSO. **(F)** Inhibition of MAK-1^{E104G} disrupts the oscillatory dynamic localization of LifeAct-
798 GFP. All observations were made multiple times (n≥15). Scale bars 5 μm.

799 **Figure 2. Actin focalizes to the tips of the interactings cells in an oscillatory manner.**
800 **(A)** Oscillatory dynamic localization of actin fusion aster at the cell tips of the interacting cells
801 with LifeAct-GFP (strain 754). Similar observations were made multiple times (n=10) **(B)**
802 Lifeact-GFP co-localization with dsRed-SO during the interaction of fusing cells in the
803 heterokaryon created with strains 754 and N1-30. **(C)** LifeAct-GFP localization in a non-
804 interacting cell during vegetative growth (strain 754). Similar observations were made multiple
805 times (n=10). Scale bars 5 μm

806 **Figure 3. Activity inhibition of MAK-2 disrupts the SO dynamic localization and**
807 **mislocalizes actin around the cell membrane**. (A) Oscillatory localization of SO-GFP during
808 cell fusion in a MAK-2^{Q100A} background (strain 911) with the addition of DMSO. (B) Inhibition
809 of MAK-2^{Q100A} disrupts the oscillatory dynamic localization of SO-GFP. (C) Oscillatory
810 localization of LifeAct-GFP during cell fusion in a MAK-2^{Q100A} background (strain 915) with
811 the addition of DMSO. (D) Inhibition of MAK-2^{Q100A} disrupts the oscillatory dynamic

812 localization of LifeAct-GFP. All observations were made multiple times (n≥10). Scale bars 5
813 μm.

814 **Figure 4. Inhibition of actin assembly disrupts the MAK-2/SO dynamic localization. (A)**
815 Inhibition of actin with latrunculin A (Lat A) disrupts the localization of MAK-2-GFP (strain 865)
816 **(B)** Inhibition of actin with Lat A disrupts the localization of SO-GFP (strain 874). **(C)** Inhibition
817 of RAC-1 with RAC-1 inhibitor (NSC23766) disrupts the localization of MAK-2-GFP (strain
818 865) **(D)** Inhibition of RAC-1 with RAC-1 inhibitor disrupts the localization of SO-GFP (strain
819 874). All observations were made multiple times (n≥10). Scale bars 5 μm.

820 **Figure 5. Activity inhibition of MAK-1 results in RAC-1 inactivation while MAK-2**
821 **inhibition results in RAC-1 mislocalization. (A)** Localization of the CRIB-GFP reporter
822 during cell fusion in a MAK-1^{E104G} background (strain 943) with the addition of DMSO. **(B)**
823 Inhibition of MAK-1^{E104G} disrupts CRIB-GFP localization during cell fusion. **(C)** Localization
824 of the CRIB-GFP reporter during cell fusion in a MAK-2^{Q100A} background (strain 949) with the
825 addition of DMSO. **(D)** Inhibition of MAK-2^{Q100A} results in mislocalization of the CRIB-GFP
826 during cell fusion. **(E)** Inhibition of MAK-2^{Q100A} results in mislocalization of the CRIB-GFP
827 during cell fusion, and subsequent addition of the RAC-1 inhibitor results in disruption of the
828 CRIB reporter. Comparable observations were made multiple times (n≥10). Scale bars 5 μm.

829 **Figure 6. Inhibition of either MAK-1 or RAC-1 does not affect actin localization in**
830 **vegetative growth. (A)** Quantification of cell elongation in cells treated either with DMSO,
831 ATP-analog (MAPK inhibitor) or RAC-1 inhibitor. No significant differences are observed
832 between all tests (n≥25). **(B)** Upper panel: localization of the CRIB-GFP reporter in non-
833 interacting cells before and after addition of DMSO in a MAK-1^{E104G} background (strain 943).
834 Bottom panel: localization of the CRIB-GFP reporter in cells before and after inhibition of
835 MAK-1^{E104G}. **(C)** Upper panel: localization of the CRIB-GFP reporter in non-interacting cells
836 before and after addition of DMSO in a MAK-2^{Q100A} background (strain 949). Bottom panel:
837 localization of the CRIB-GFP reporter in cells before and after inhibition of MAK-2^{Q100A} **(D)**
838 Upper panel: localization of LifeAct-GFP in non-interacting cells before and after addition of
839 DMSO in a MAK-1^{E104G} background (strain 869). Bottom panel: localization of LifeAct-GFP
840 in cells before and after inhibition of MAK-1^{E104G}. **(E)** Upper panel: localization of LifeAct-GFP
841 in non-interacting cells before and after addition of DMSO in a MAK-2^{Q100A} background (strain
842 915). Bottom panel: localization of LifeAct-GFP in cells before and after inhibition of MAK-
843 2^{Q100A}. Similar observations were made multiple times (n≥5). Scale bars 5 μm.

844 **Figure 7. RAC-1 and MAK-1 acts within the same pathway. (A)** Quantification of twisting
845 and normal growth in cell fusion during partial inhibition of RAC-1. Control (H_2O) and 25 μM
846 of RAC-1 inhibitor are shown (n≥100). Representative images of both phenotypes are shown
847 at the right. **(B)** Quantification of polarity growth defects when RAC-1 is partially inhibited
848 during cell fusion. Control (H2O) and 25 μM (NSC23766), in media with/without Ca^{2+} and with
849 Δso strain as a control. Significant differences (***, p<0.001) were observed between the
850 partial inhibition and the control only in the presence of Ca^{2+}.

851 **Figure 8. MAK-1 is upstream of RAC-1. (A)** Localization of CRIB-GFP when cells establish
852 physical contact in a MAK-1^{E104G} background (strain 943), when treated with DMSO. **(B)**
853 Localization of CRIB-GFP during inhibition of MAK-1^{E104G} after cells established physical
854 contact. (*) to point the cell fusion event and signal dissapearence. **(C)** Localization of MAK-
855 1-GFP in a wild-type interaction when cells established physical contact (strain MW513). **(D)**
856 Localization of MAK-1-GFP when RAC-1 is fully inhibited with NSC23766 (100 μM). Similar
857 observations were made multiple times (n=10) Scale bars 5 μm.

858 **Figure 9. Proposed model of MAK-1/MAK-2 regulation during cell fusion**. **A)** During
859 chemotropic growth toward a fusion partner, MAK-1 activates RAC-1, which in turn drives actin
860 polymerization and formation of a focused actin aster at the leading tip. This actin/RAC-1
861 complex supports polarized exocytosis and directed growth. In parallel, MAK-2 defines the
862 position of this complex by orienting RAC-1 and the actin aster toward the partner cell. **B)**
863 When MAK-1^{E104G} activity is blocked, RAC-1 becomes inactive and detaches from the
864 membrane, the actin aster collapses, and growth stops. **C)** When MAK-2^{Q100A} activity is
865 blocked, RAC-1 remains active at the cortex but shifts to ectopic positions around the plasma
866 membrane, and growth loses direction.

867

868 **Supplementary information**

869 **Supplementary figures**

870 **Figure S1. Characterization of MAK-1^{E104G} strains. (A)** Graphical representation of the
871 knock-in construct integrated in the genome of the transformant strains. Arrows indicate
872 BamH1 cutting sites and the bands that are generated. **(B)** Southern blot of the positive strains
873 obtained after transformation and crossing with the wild-type strain. DNA was treated with
874 BamH1 before hybridization with the membrane **(C)** Macroscopic phenotype of wild type and
875 MAK-1^{E104G} (strain 849) in presence of DMSO or ATP-analog. Similar observations were

876 made on strains 848, 850 and 851 (same genotype than 849). **(D)** Quantification of tropic
877 interactions and germination of MAK-1^{E104G} strain in presence of DMSO or the ATP-analog
878 (n>100).

879 **Figure S2. Oscillatory recruitment of MAK-2/SO and actin is disrupted after MAK-1**
880 **inhibition during hyphal fusion. (A)** Localization of MAK-2-GFP during inhibition of MAK-
881 1^{E104G} (strain 865) in a hyphal fusion. **(B)** Localization of SO-GFP during inhibition of MAK-
882 1^{E104G} (strain 874) in a hyphal fusion. **(C)** Localization of LifeAct-GFP during inhibition of MAK-
883 1^{E104G} (strain 869) in a hyphal fusion. Similar observations were made multiple times (n>5).
884 Scale bars: 5 µm.

885 **Figure S3. Quantifications of signal intensity during cell fusion. (A)** Lifeact relative
886 intensity ratio between the signal localized at 3 µm within the apex of the cell and the
887 cytoplasm, from the images shown in figure 2A. **(B)** Lifeact relative intensity ratio between the
888 signal localized at 3 µm within the apex of the cell and the cytoplasm, from the images shown
889 in figure 2B. **(C)** SO relative intensity ratio between the signal localized at 3 µm within the apex
890 of the cell and the cytoplasm, from the images shown in figure 2B. **(D)** Combination of data
891 extracted from graphs B and C from the left cell of the image, indicating a asynchronous
892 oscillation.

893 **Figure S4. Characterization of MAK-2^{Q100A} strains. (A)** Graphical representation of the
894 knock-in construct integrated in the genome of the transformant strains. Arrows indicate
895 BamH1 cutting sites and the bands that are generated. **(B)** Southern blot of the positive strains
896 obtained after transformation and crossing with the wild-type strain. DNA was treated with
897 BamH1 before hybridization with the membrane. **(C)** Macroscopic phenotype of wild type and
898 MAK-2^{Q100A} (strain 898) in presence of DMSO or the ATP-analog. Similar observations were
899 made on strains AS899, AS900 and AS901 (same genotype as 898). **(D)** Quantification of
900 tropic interactions and germination of MAK-2^{Q100A} strain in presence of DMSO or the ATP-
901 analog (n>100).

902 **Figure S5. Actin and MAK-2 inhibition effect on SO/actin dynamics. (A)** Localization of
903 SO-GFP during MAK-2^{Q100A} (strain 912) inhibition on interacting cells. **(B)** Localization of
904 LifeAct-GFP during MAK-2^{Q100A} (strain 915) inhibition on interacting cells. **(C)** Effect of the actin
905 inhibitor latrunculin A on actin assembly in LifeAct-GFP localization (strain 754). **(D)** Effect of
906 RAC-1 inhibition on LifeAct-GFP (strain 869) localization during cell fusion. Similar
907 observations were made multiple times (n>5).

908 **Figure S6. Effect of RAC-1 inhibition on CRIB-GFP localization and actin assembly on**
909 **strain. (A)** CRIB-GFP localization after RAC-1 inhibition (NSC23766) during cell fusion. **(B)**
910 Relative intensity ratio between the signal localized at 3 µm within the apex or in the germ
911 tube of the cell and the cytoplasm, from the images shown in figure 5C. At the left *y-axis* is
912 represented the apex/cytop signal (red and dark blue) and in the right *y-axis* blue) and in the
913 right *y-axis* is represented the germ tube plasma membrane/cytop signal (light blue and
914 orange). (C) Actin localization and organization in Δ*mak-1* (strain NCU09482).

915 **Table S1. List of strains used in this study.**

Strain	Genotype	Source
N1-01 (FGSC #2489)	Wild type, *Mat A*	FGSC
N1-02 (FGSC #988)	Wild type, *Mat a*	FGSC
N1-03 (FGSC #6103)	*his-3; Mat A*	FGSC
N1-05 (FGSC #9720)	Δ*mus-52::bar+, his-3*, mat A	FGSC
N1-06 (FGSC #9719)	Δ*mus-52::bar+*, mat a	FGSC
NCU09482 (FGSC #11326)	Δ*mak-1*::*hph*	FGSC
714	*his-3*$^{+}$*::Ptef-1-so-gfp, mat A.*	This study
754	*his-3*$^{+}$*::Ptef-1-Lifeact-gfp; Δmus-51::bar+; mat A*	[18]
758	*his-3*$^{+}$*::Ptef-1-mak-2-mCherry*	This study
843	*his-3*$^{+}$*::Ptef-1-dsred-so; Mat A*	This study

848	*mak-1:: mak-1^{E104G}-hph, his-3; Mat a*	This study
849	*mak-1:: mak-1^{E104G}-hph; Mat a*	This study
850	*mak-1:: mak-1^{E104G}-hph; Mat a*	This study
851	*mak-1:: mak-1^{E104G}-hph; bar+::mus52; Mat A*	This study
865	*mak-1::mak-^{E104G}-hph; his-3::Ptef-1-mak-2-gfp; mat A*	This study
869	*mak-1:: mak-1^{E104G}-hph; his-3::Ptef-1-lifeact-gfp; mat A*	This study
874	*mak-1::mak-1^{E104G}-hph; his-3::Ptef-1-so-gfp; mat A*	This study
882	*Pmak-2-mak-2::Ptef-1-mak-2^{Q100A}-hph; his-3-, bar+::mus52; mat A*	This study
891	*mak-1::hph, his-3::Ptef-1-lifeact-gfp mat a*	This study
898	*Pmak-2-mak-2::Ptef-1-mak-2^{Q100A}-hph; mat a*	This study
899	*Pmak-2-mak-2::Ptef-1-mak-2^{Q100A}-hph; mat a*	This study
900	*Pmak-2-mak-2::Ptef-1-mak-2^{Q100A}-hph; mat a*	This study
901	*Pmak-2-mak-2::Ptef-1-mak-2^{Q100A}-hph; mat a*	This study
911	*Pmak-2-mak-2::Ptef-1-mak-2^{Q100A}-hph; his-3+::Ptef-1-so-gfp*	This study
915	*Pmak-2-mak-2::Ptef-1-mak-2^{Q100A}-hph; his-3+::Ptef-1-lifeact-gfp*	This study
927	*Pccg1::crib^cla-4-gfp::bar+ Mat A*	[43]

943	*mak-1::-mak-1^{E104G}-hph; Pccg1::crib^cla-4-gfp::bar+*	This study
949	*Pmak-2-mak-2::Ptef-1-mak-2^{Q100A}-hph; Pccg1::crib^cla-4-gfp::bar+*	This study

916

917

918 **Table S2. List of primers used in this study.**

N	Name	Nucleotide sequence 5' -------> 3'
1419	SO-Ascl-Fw	aatgtaggcgcgcccatgtctcgatcccgcggtgttc
1420	SO-Xbal-Rv	aatgtatctagactaatgcccatactccaaatgcggc
1487	mak-2 Q100G R	gagccagcacgcgatcatacgccgatgagatacacttcgttga
1488	mak-2 Q100G F	tcaacgaagtgtatctcatcggcgtatgatcgcgtgctggctc
1489	mak2 5strichF--pRS	gtaacgccagggttttcccagtcacgacgtctctctggttgttctgttcgga
1490	mak2 5srichR --tef Promotor	tagttcagtggtcacgggatatccaactacttcacccttcacaca
1492	MAK-2-Pr1.Rv	tcacctcataatctcctggtagatcaactgc

1304	Mak1.knockin.1	gtaacgccagggttttcccagtcacgacgcgagacctatctctacggcggtacgtcatggctcat
1305	Mak1.knockin.2	atccacttaacgttactgaaatcaaacattctttttggctttttgtactaatctgg
1306	Mak1.knockin.3	gctccttcaatatcatcttctgtgaacgccgacgccatgcag
1307	Mak1.knockin.4	gcggataacaatttcacacaggaaacagctcctctctctctccgtcgtcgcc
82	HPH F	gtcggagacagaagatgatattgaaggagc
83	HPH R	gttggagatttcagtaacgttaagtggat

919

920 **Table S3. List of plasmids used in this study**.

Number	Plasmid
723	*Ptef-1-dsRed-so*
846	*Ptef-1-mak-2q100a*
738	*mak-1-e104g*

921

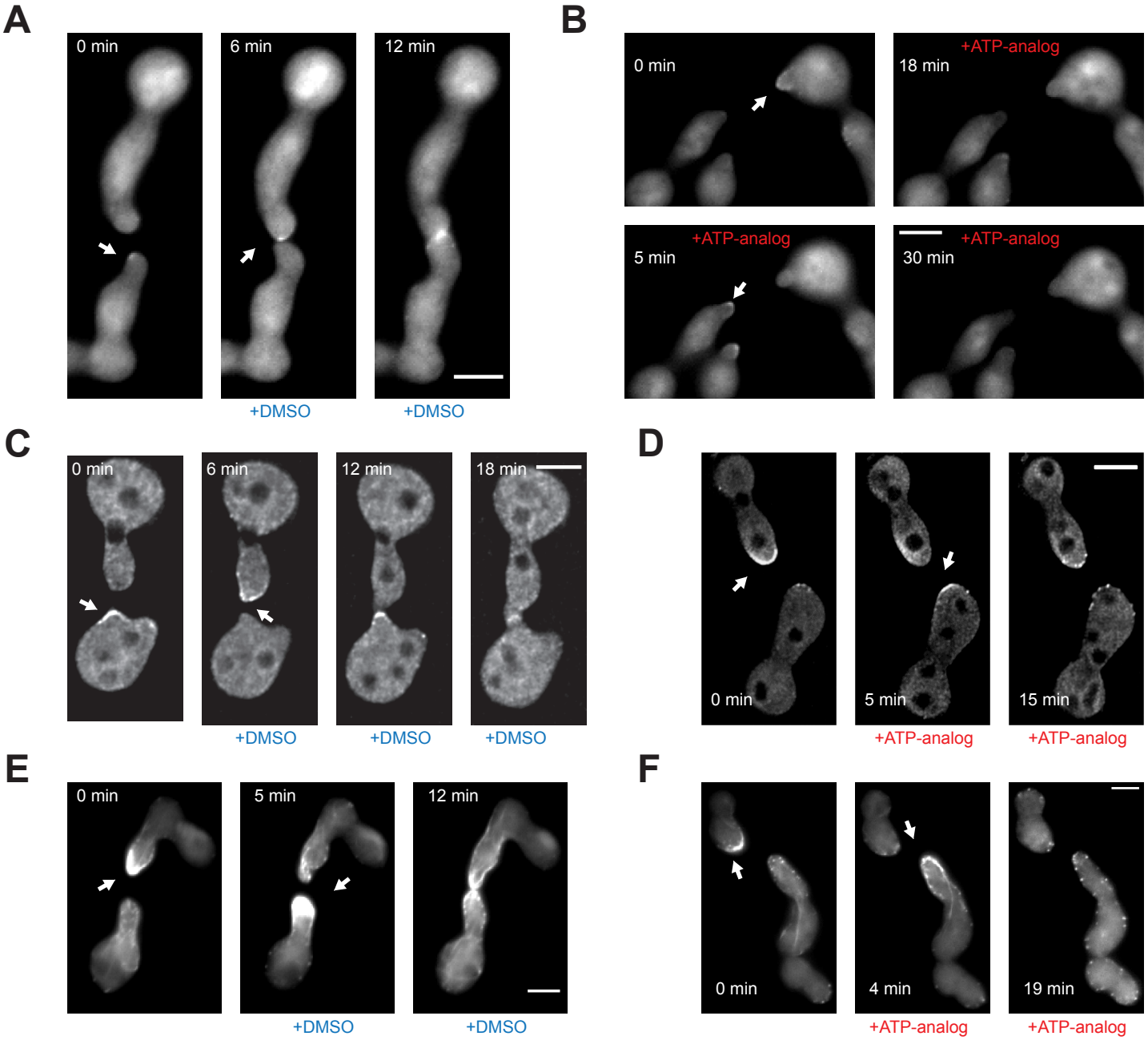
A
0 min
6 min
12 min
+DMSO
+DMSO
B
0 min
+ATP-analog
18 min
+ATP-analog
5 min
+ATP-analog
30 min
C
0 min
6 min
12 min
18 min
+DMSO
+DMSO
+DMSO
D
0 min
5 min
15 min
+ATP-analog
+ATP-analog
E
0 min
5 min
12 min
+DMSO
+DMSO
F
0 min
4 min
19 min
+ATP-analog
+ATP-analog

Figure 1

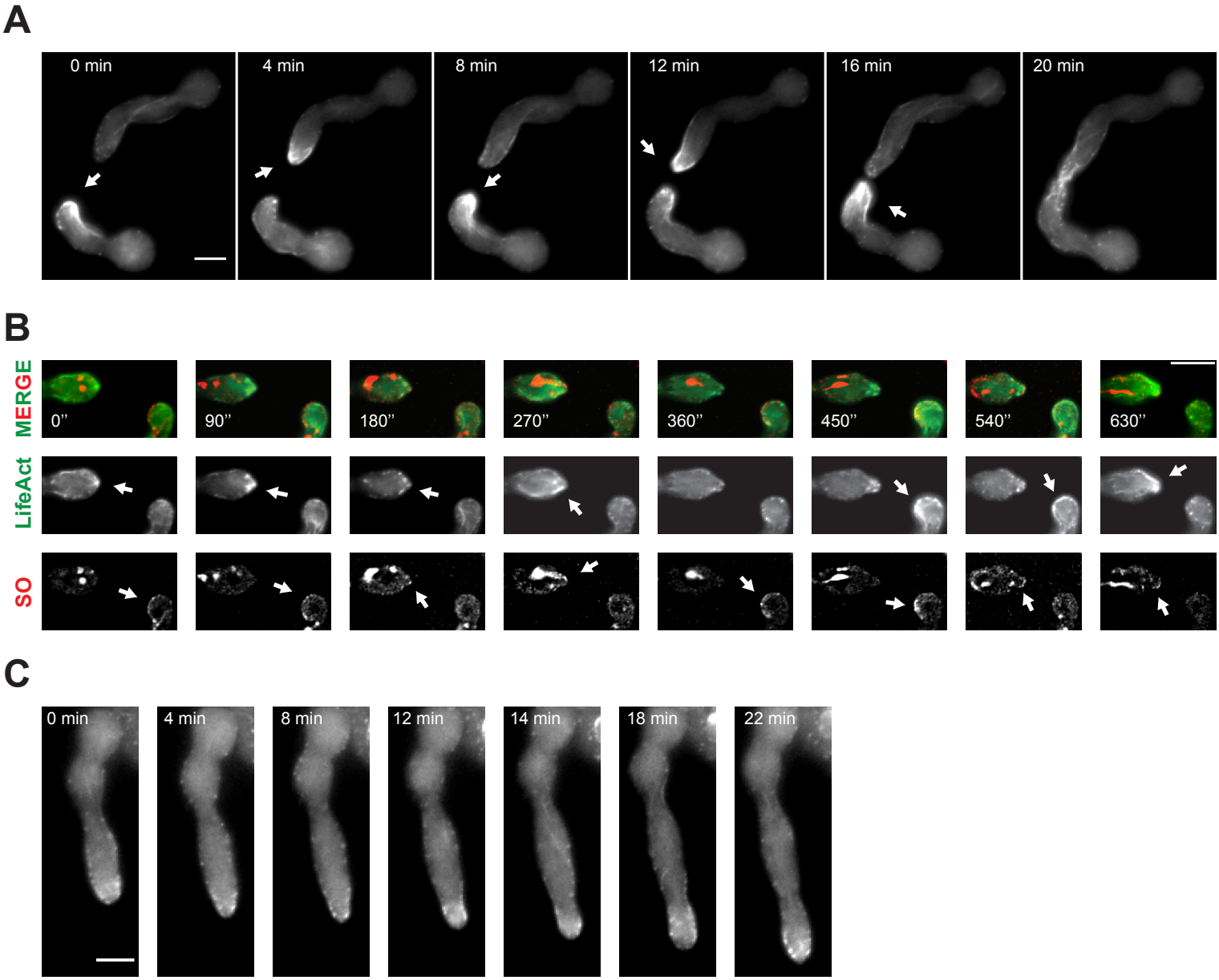
A
0 min
4 min
8 min
12 min
16 min
20 min
B
MERGE
LifeAct
SO
0''
90''
180''
270''
360''
450''
540''
630''
C
0 min
4 min
8 min
12 min
14 min
18 min
22 min

Figure 2

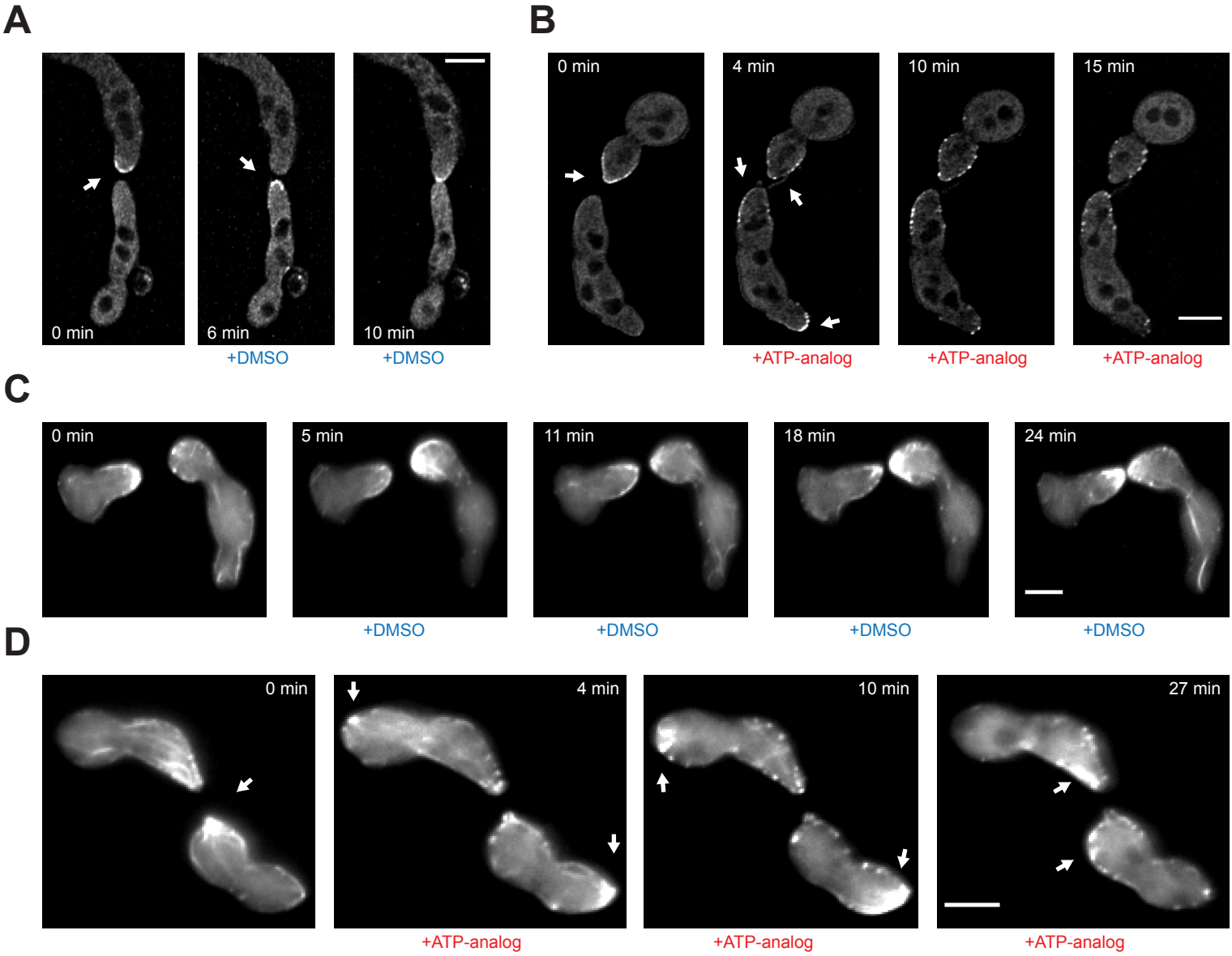
A
0 min
6 min
10 min
+DMSO
+DMSO
B
0 min
4 min
10 min
15 min
+ATP-analog
+ATP-analog
+ATP-analog
C
0 min
5 min
11 min
18 min
24 min
+DMSO
+DMSO
+DMSO
+DMSO
D
0 min
4 min
10 min
27 min
+ATP-analog
+ATP-analog
+ATP-analog

Figure 3

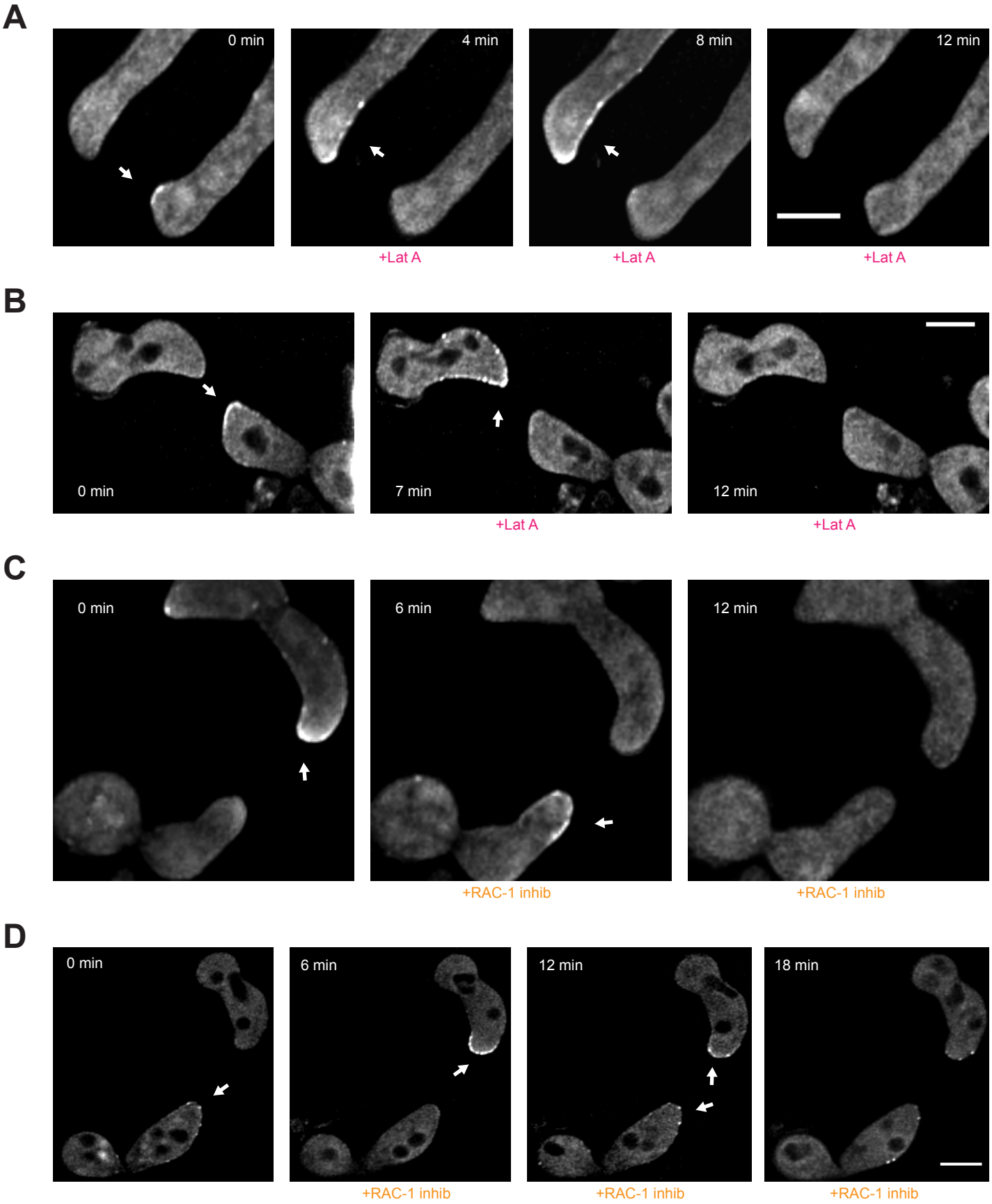
A
0 min
4 min
8 min
12 min
+Lat A
+Lat A
+Lat A
B
0 min
7 min
12 min
+Lat A
+Lat A
C
0 min
6 min
12 min
+RAC-1 inhib
+RAC-1 inhib
D
0 min
6 min
12 min
18 min
+RAC-1 inhib
+RAC-1 inhib
+RAC-1 inhib

Figure 4

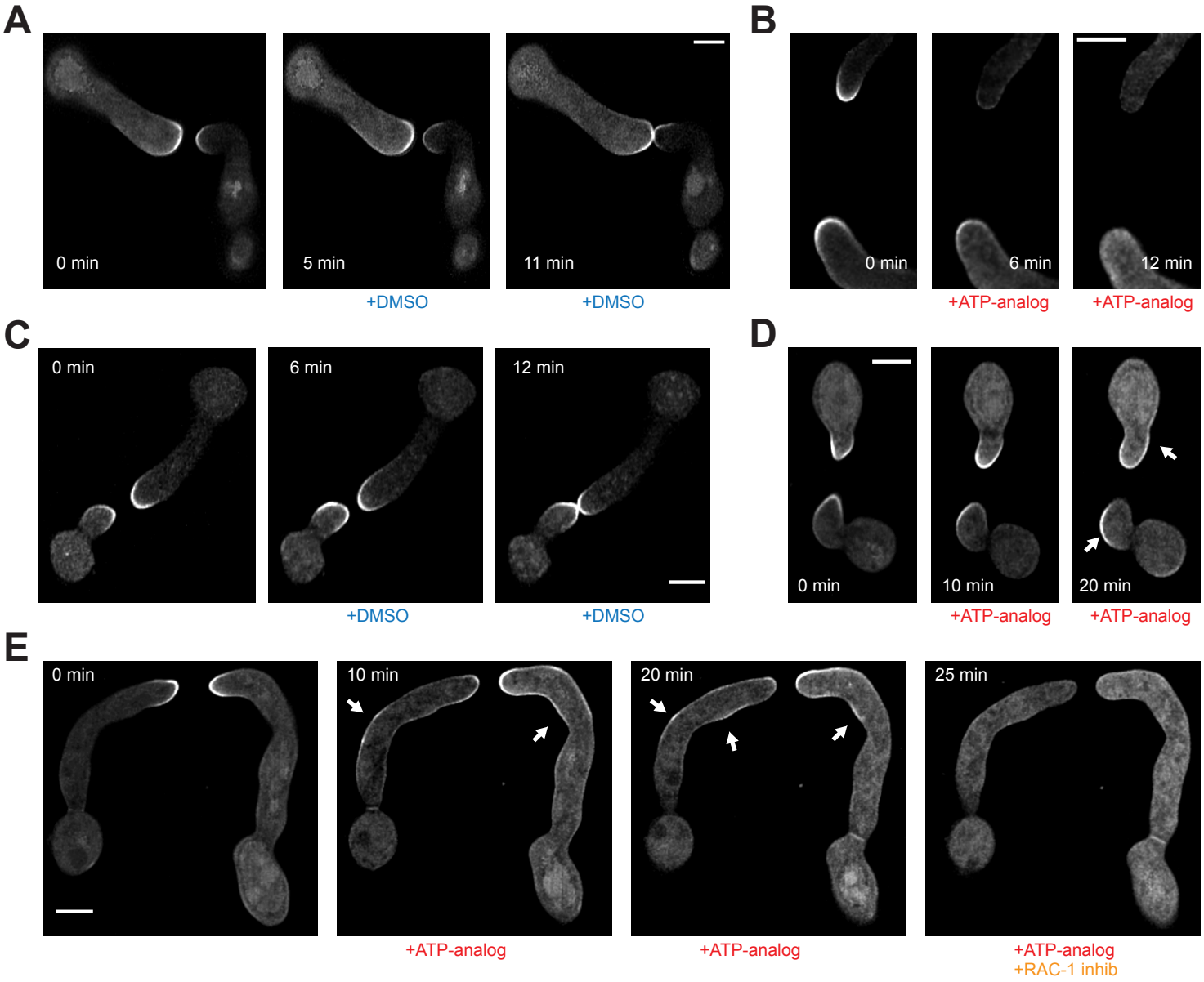
A
0 min
5 min
11 min
+DMSO
+DMSO
B
0 min
6 min
12 min
+ATP-analog
+ATP-analog
C
0 min
6 min
12 min
+DMSO
+DMSO
D
0 min
10 min
20 min
+ATP-analog
+ATP-analog
E
0 min
10 min
20 min
25 min
+ATP-analog
+ATP-analog
+ATP-analog
+RAC-1 inhib

Figure 5

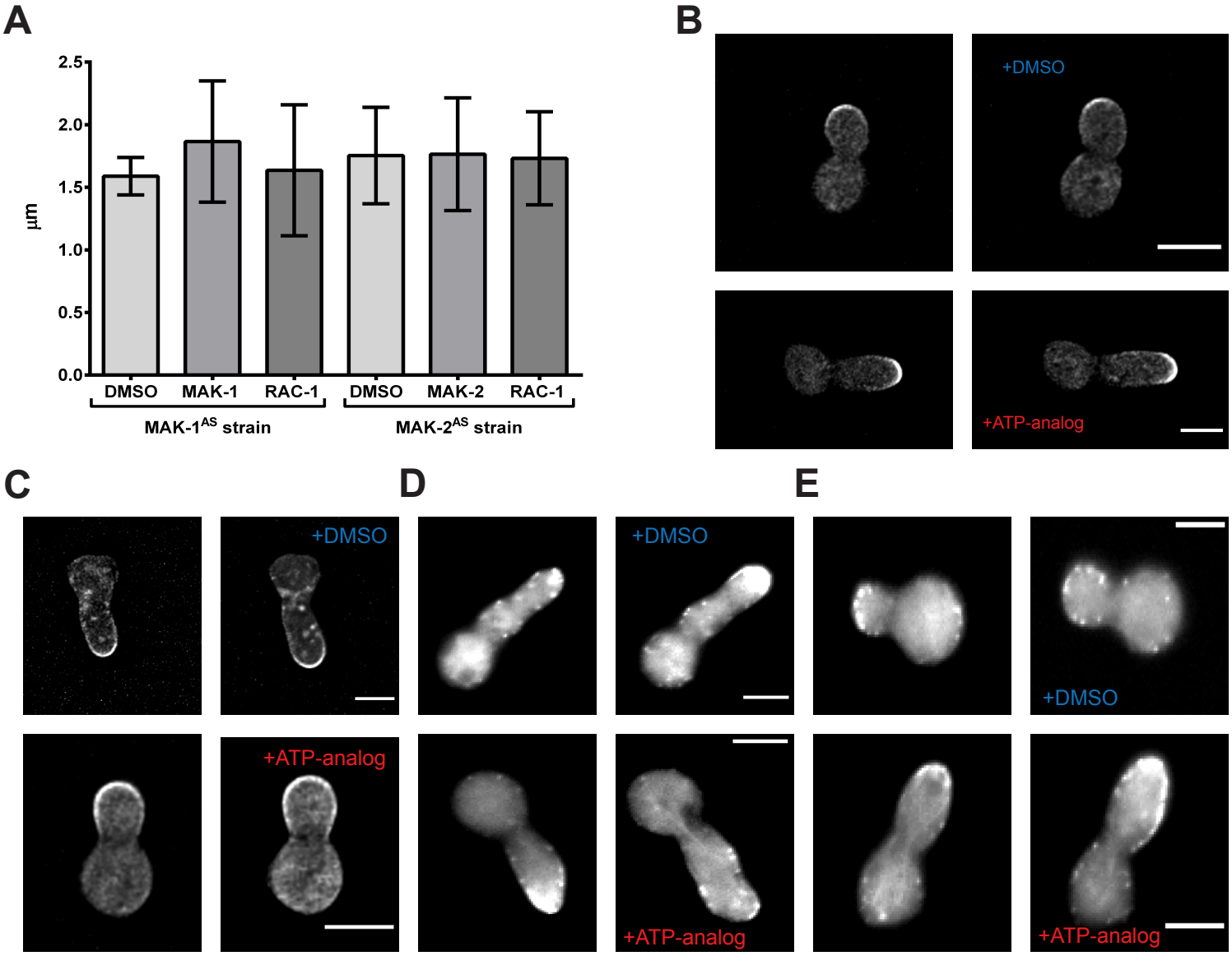
A
2.5
2.0
1.5
1.0
0.5
0.0
µm
DMSO
MAK-1
RAC-1
DMSO
MAK-2
RAC-1
MAK-1AS strain
MAK-2AS strain
B
+DMSO
+ATP-analog
C
+DMSO
+ATP-analog
D
+DMSO
+ATP-analog
E
+DMSO
+ATP-analog

Figure 6

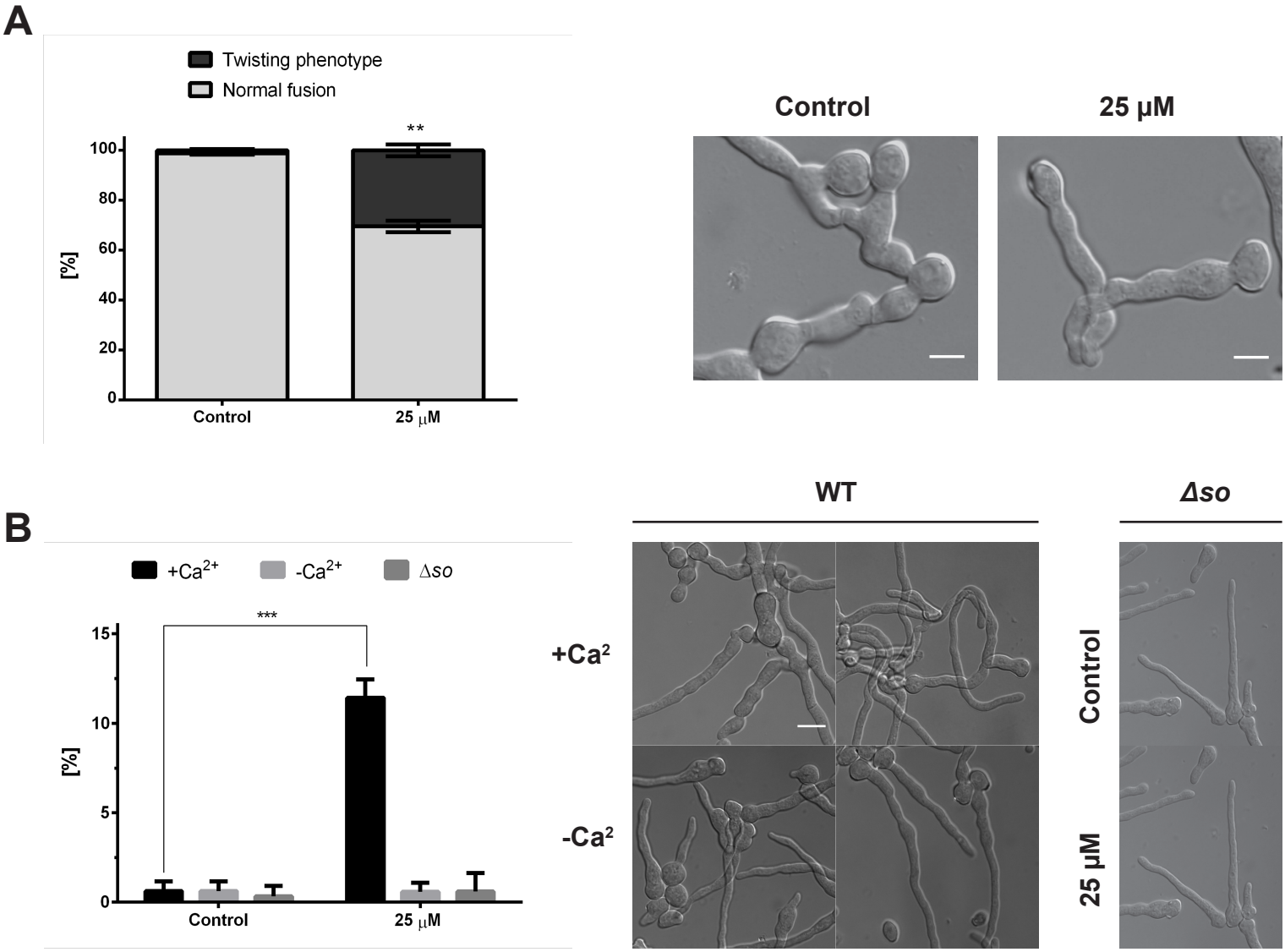
A
Twisting phenotype
Normal fusion
**
100
80
60
40
20
0
[%]
Control
25 μM
Control
25 μM
B
+Ca2+
-Ca2+
Δso
***
15
10
5
0
[%]
Control
25 μM
WT
Δso
+Ca2
-Ca2
Control
25 μM

Figure 7

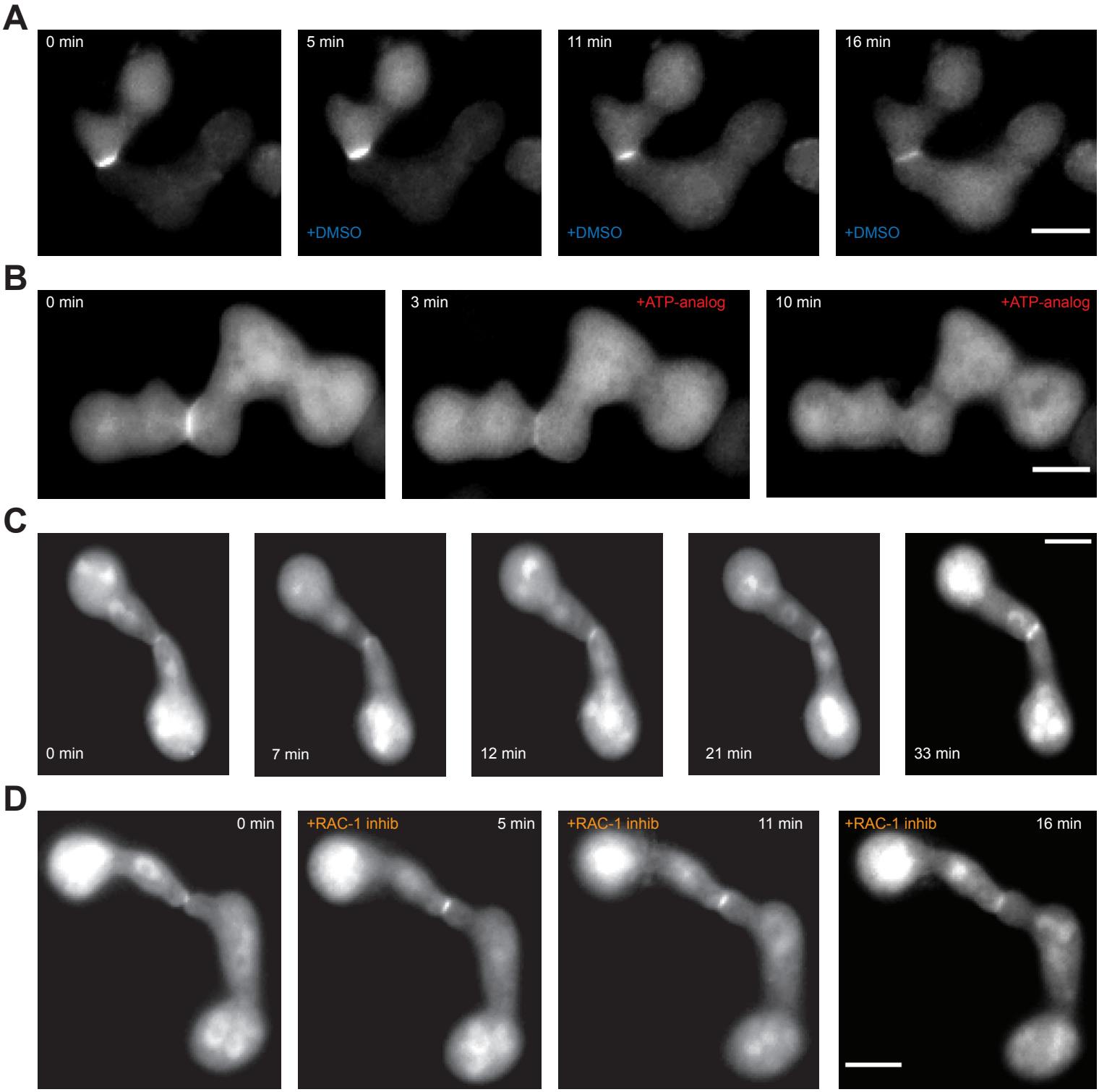
A
0 min
5 min
+DMSO
11 min
+DMSO
16 min
+DMSO
B
0 min
3 min
+ATP-analog
10 min
+ATP-analog
C
0 min
7 min
12 min
21 min
33 min
D
0 min
+RAC-1 inhib
5 min
+RAC-1 inhib
11 min
+RAC-1 inhib
16 min

Figure 8

A

Wild type

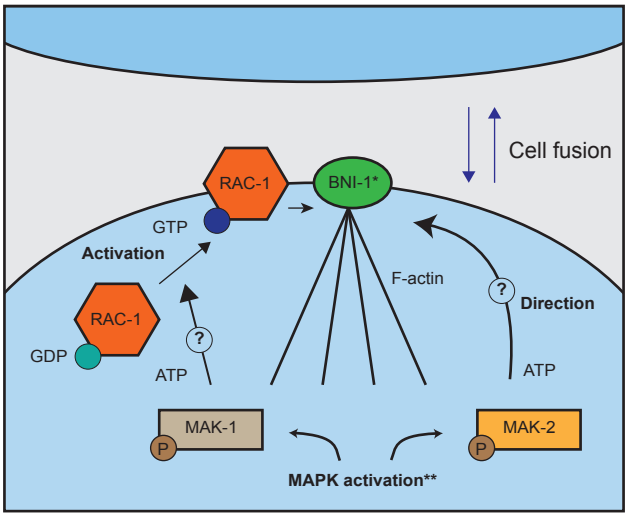

*Or another unknown actin nucleator
** Two independent three-tiered MAPK cascade activation

B

MAK-1^{E104G} Inhibition

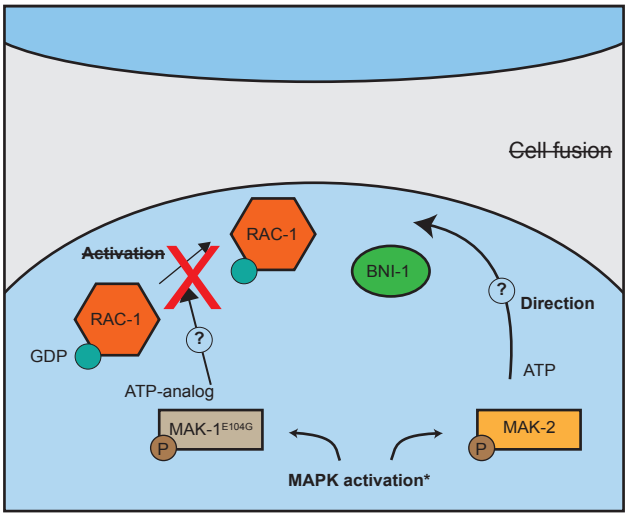

* Two independent three-tiered MAPK cascade activation

C

MAK-2^{Q100A} Inhibition

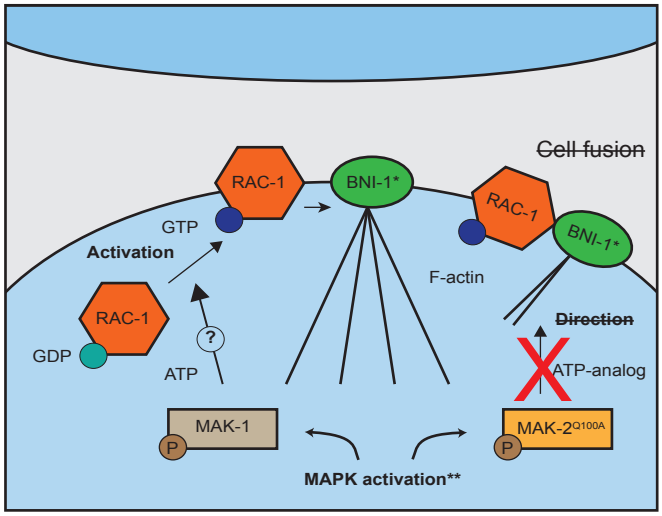

*Or another unknown actin nucleator
** Two independent three-tiered MAPK cascade activation

Figure 9